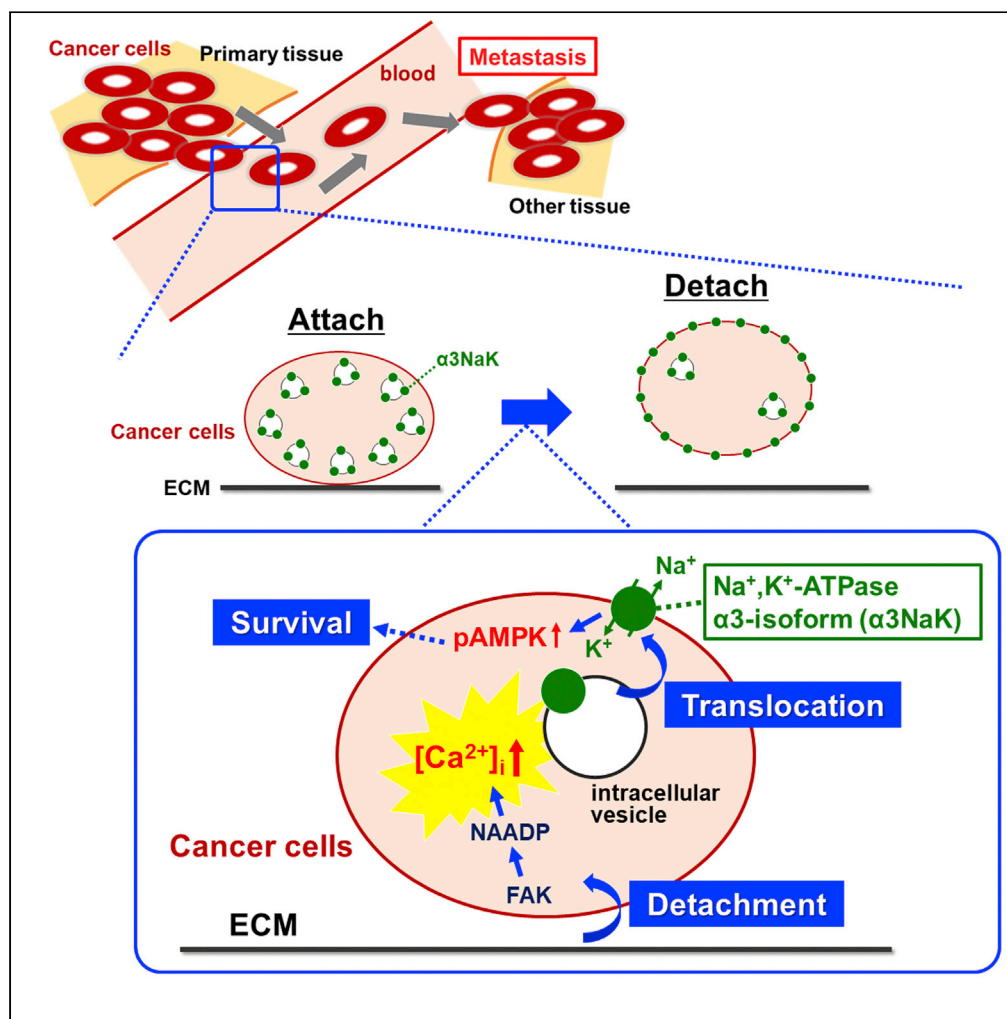


Article

Survival of detached cancer cells is regulated by movement of intracellular Na^+, K^+ -ATPase

Takuto Fujii,
Takahiro Shimizu,
Mizuki Katoh, ...,
Tsutomu Fujii,
Hiroshi
Takekuma, Hideki
Sakai

sakaih@pha.u-toyama.ac.jp

Highlights

Na^+, K^+ -ATPase $\alpha 3$ -isoform ($\alpha 3\text{NaK}$) is localized in cytoplasm of attached cancer cells

Intracellular $\alpha 3\text{NaK}$ is moved to plasma membrane (PM) upon the cell detachment

FAK and NAADP-dependent Ca^{2+} response is involved in the translocation of $\alpha 3\text{NaK}$

Activation of AMPK associated with the PM- $\alpha 3\text{NaK}$ contributes to the cell survival

Fujii et al., iScience 24, 102412
May 21, 2021 © 2021 The
Author(s).
<https://doi.org/10.1016/j.isci.2021.102412>

Article

Survival of detached cancer cells
is regulated by movement of intracellular
 Na^+, K^+ -ATPase

Takuto Fujii,¹ Takahiro Shimizu,¹ Mizuki Katoh,¹ Shushi Nagamori,² Keiichi Koizumi,³ Junya Fukuoka,^{4,9} Yoshiaki Tabuchi,⁵ Akira Sawaguchi,⁶ Tomoyuki Okumura,⁷ Kazuto Shibuya,⁷ Tsutomu Fujii,⁷ Hiroshi Takeshima,⁸ and Hideki Sakai^{1,10,*}

SUMMARY

Beginning of metastasis, cancer cells detach from the primary tumor and they can survive even under loss of anchorage; however, the detachment-elicited mechanisms have remained unknown. Here, we found that Na^+, K^+ -ATPase $\alpha 3$ -isoform ($\alpha 3\text{NaK}$) in human cancer cells is dynamically translocated from intracellular vesicles to the plasma membrane when the attached cells are detached and that this mechanism contributes to the survival of the detached (floating) cancer cells. $\alpha 3\text{NaK}$ was detected in the plasma membrane of floating cancer cells in peritoneal fluids of patients, while it was in the cytoplasm of the cells in primary tumor tissues. On cancer cell detachment, we also found the focal-adhesion-kinase-dependent Ca^{2+} response that induces the $\alpha 3\text{NaK}$ translocation via nicotinic acid adenine dinucleotide phosphate pathway. Activation of AMP-activated protein kinase was associated with the translocated $\alpha 3\text{NaK}$ in the plasma membrane. Collectively, our study identifies a unique mechanism for survival of detached cancer cells, opening up new opportunities for development of cancer medicines.

INTRODUCTION

Cancer metastasis is the major cause of mortality in patients with cancer and responsible for up to 90% of cancer death (Seyfried and Huysentruyt, 2013). During the metastatic process, the detached cancer cells from the primary tumor tissue spread to different sites through blood/lymphatic vessels, then settle, and grow at a site other than the primary site. Malignant floating cancer cells can evade the detachment-induced cell death (DICD) and survive even under the loss of anchorage condition (Buchheit et al., 2012; Guadamillas et al., 2011), whereas normal epithelial cells undergo cell death when they lack their anchorage to the extracellular matrix (ECM). Thus, the anchorage-independent survival is a unique feature of metastatic cancer cells. So far, the AMP-activated protein kinase (AMPK) has been reported to have an essential role in resistance to DICD by activation (phosphorylation) of AMPK (Sundaraman et al., 2016; Jin et al., 2018). However, cell detachment-elicited mechanisms evading DICD have not been fully established.

Na^+, K^+ -ATPase is mainly located in the plasma membrane (PM) and is a crucial enzyme that regulates membrane potential and cellular ion homeostasis in almost all mammalian cells. On the other hand, abnormal expression of Na^+, K^+ -ATPase has been reported in various cancers (Durlacher et al., 2015). A number of *in vitro* and *in vivo* studies have shown that cardiac glycosides, inhibitors of Na^+, K^+ -ATPase, can block cancer cell growth (Calderón-Montaño et al., 2014; Diederich et al., 2017; Fujii et al., 2018). In addition, chemical screening showed that some cardiac glycosides exhibited a potent inhibitory effect on the resistance to anoikis (or cell-detachment-induced apoptosis) of cancer cells (Liu et al., 2008). Therefore, Na^+, K^+ -ATPase is thought to be a therapeutic target for cancer treatment.

Na^+, K^+ -ATPase $\alpha 3$ -isoform ($\alpha 3\text{NaK}$) is highly expressed in the PM of neuronal cells and involved in restoring neuronal membrane potential after depolarization and for maintaining neuronal excitability (Holm and Lykke-Hartmann, 2016). On the other hand, $\alpha 3\text{NaK}$ has been reported to be abnormally expressed in the cells of human colorectal and liver cancers (Sakai et al., 2004; Shibuya et al., 2010). In addition, the expression of $\alpha 3\text{NaK}$ in intracellular compartments, but not in the PM, was reported in colon and pancreas

¹Department of Pharmaceutical Physiology, Faculty of Pharmaceutical Sciences, University of Toyama, Toyama 930-0194, Japan

²Department of Laboratory Medicine, The Jikei University School of Medicine, Tokyo 105-8461, Japan

³Laboratory of Drug Discovery and Development for Pre-disease, Section of Host Defences, Division of Bioscience, Institute of Natural Medicine, University of Toyama, Toyama 930-0194, Japan

⁴Laboratory of Pathology, Toyama University Hospital, Toyama 930-0194, Japan

⁵Division of Molecular Genetics Research, Life Science Research Center, University of Toyama, Toyama 930-0194, Japan

⁶Department of Anatomy, Ultrastructural Cell Biology, Faculty of Medicine, University of Miyazaki, Miyazaki 889-1692, Japan

⁷Department of Surgery and Science, Faculty of Medicine, University of Toyama, Toyama 930-0194, Japan

⁸Department of Biological Chemistry, Graduate School of Pharmaceutical Sciences, Kyoto University, Kyoto 606-8501, Japan

⁹Present address: Department of Pathology, Nagasaki University Graduate School of Biomedical Sciences, Nagasaki 852-8523, Japan

¹⁰Lead contact

*Correspondence: sakaih@pha.u-toyama.ac.jp
<https://doi.org/10.1016/j.isci.2021.102412>



cancer cell lines (Yang et al., 2009, 2014). However, the pathophysiological roles of the intracellular $\alpha 3\text{NaK}$ in cancer cells are poorly understood.

In the present study, we found that $\alpha 3\text{NaK}$ is localized in the intracellular vesicles in attached cancer cells and that the vesicles are translocated to the PM by the loss of cell-ECM adhesion. Interestingly, the translocation of $\alpha 3\text{NaK}$ contributed to the survival of detached cancer cells.

RESULTS

Loss of cell adhesion induces dynamic trafficking of intracellular $\alpha 3\text{NaK}$ to the PM

The expression of $\alpha 3\text{NaK}$ in human cancer tissues was examined by using a human tissue microarray with an anti- $\alpha 3\text{NaK}$ antibody. The significant expression of $\alpha 3\text{NaK}$ was observed in a variety of cancers, and percentage of the $\alpha 3\text{NaK}$ -positive tissues was especially high in colorectal (94%) and gastric (83%) cancers (Figures 1A and S1). In immunohistochemistry of the colorectal cancer and adjacent noncancer tissues from a patient, $\alpha 3\text{NaK}$ was predominantly expressed in the cytoplasm of the cancer cells, but no significant expression was observed in the noncancer cells (Figure 1B).

During the process of peritoneal dissemination, advanced gastric and colorectal cancer cells detach from their primary locations and thereafter survive even upon anchorage loss. Resistance to the DICD is a crucial factor for the development of peritoneal dissemination of human gastric cancer cells (Yawata et al., 1998). Here, we examined the localization of $\alpha 3\text{NaK}$ in floating cancer cells in the peritoneal fluid of patients with gastric and colon cancer. Interestingly, localization of $\alpha 3\text{NaK}$ in the PM was observed in the floating gastric cancer cells which express carcinoembryonic antigen (CEA), a tumor marker of gastrointestinal malignancies (Figure 1D). In contrast, $\alpha 3\text{NaK}$ was observed only in the cytoplasm of cancer cells in the primary site from the same patient (Figure 1C). In floating colon cancer cells in the peritoneal fluid of another patient, $\alpha 3\text{NaK}$ was also found to be localized in the PM (Figure 1E). These results prompted us to hypothesize that $\alpha 3\text{NaK}$ in the cancer cells is translocated from the cytoplasm to the PM by losing the cell anchorage during metastasis.

To explore this hypothesis, we first performed *in vitro* experiments using human cancer cell lines: colorectal cancer HT-29 cells, gastric cancer MKN45 cells, and hepatocellular carcinoma HepG2 cells. Under the cell-attached condition, $\alpha 3\text{NaK}$ was detected in the cytoplasm and its localization was not overlapped with flotillin-2, a marker for the PM (Figures 1F and S2A). In addition, the localization of $\alpha 3\text{NaK}$ was different from organelle markers of the endoplasmic reticulum (ER; calnexin), Golgi body (TGN46), endosome (EEA1), lysosome (LAMP1), and mitochondria (MitoTracker) (Figure S3). Interestingly, most of the $\alpha 3\text{NaK}$ were colocalized with Rab10, a small GTPase (Stenmark, 2009), which contributes to vesicular trafficking in the cytoplasm of the cancer cells (Figures S4A and S4C). In contrast, no significant colocalization of $\alpha 3\text{NaK}$ with Rab4, 5, 7, 8, 9, or 11 was observed (Figures S4A and S4B). Electron microscopy analysis with a high-pressure freezing method showed the assembly (less than 50 nm of diameter) of $\alpha 3\text{NaK}$ underlying the PM of the cells (Figure 1G). The average number of $\alpha 3\text{NaK}$ molecule in each assembly was around 4, and the average distance of the assembly from the PM was 418 nm (Figure S5A). These results suggest that $\alpha 3\text{NaK}$ is localized in intracellular Rab10-expressing vesicles in attached cancer cells.

We next examined the changes in the localization of $\alpha 3\text{NaK}$ upon cancer cell detachment. When cancer cells were detached from the matrix of dishes by treatment with ethylenediaminetetraacetic acid (EDTA) and trypsin, the signal of $\alpha 3\text{NaK}$ was detected in the PM in which flotillin-2 was localized (Figures 1H, S2B, and S5B), suggesting that $\alpha 3\text{NaK}$ is translocated from the cytoplasm to the PM upon cell detachment. Interestingly, when the detached cells were replated on a dish, localization of $\alpha 3\text{NaK}$ in the cytoplasm was found again (Figures 1H, S2B, and S5B). Similarly, localization of Rab10 was changed from the cytoplasm to the PM upon cell detachment, and it was in the cytoplasm again after cell reattachment (Figures S4C and S4D). In addition, we performed surface biotinylation assay. In the assay, no significant bands of intracellular proteins such as the thiol oxidoreductase ERp57 and nonmuscle myosin IIA were observed in the biotinylation samples (Figure 1I), suggesting no leakage of biotin into the cytoplasm through the procedure of cell detachment. Consistent with the results in immunocytochemistry (Figures 1H and S2B), the expression level of $\alpha 3\text{NaK}$ in the PM (biotinylation samples) of detached cells was much higher than attached and reattached cells (Figures 1I and S2C). On the other hand, the expression level of Na^+, K^+ -ATPase $\alpha 1$ -isoform ($\alpha 1\text{NaK}$) in the PM of detached cells was comparable with attached and reattached cells (Figure 1I). In addition, the K^+ -transporting activity of Na^+, K^+ -ATPase in the PM of the cells was measured using $^{86}\text{Rb}^+$ as a K^+

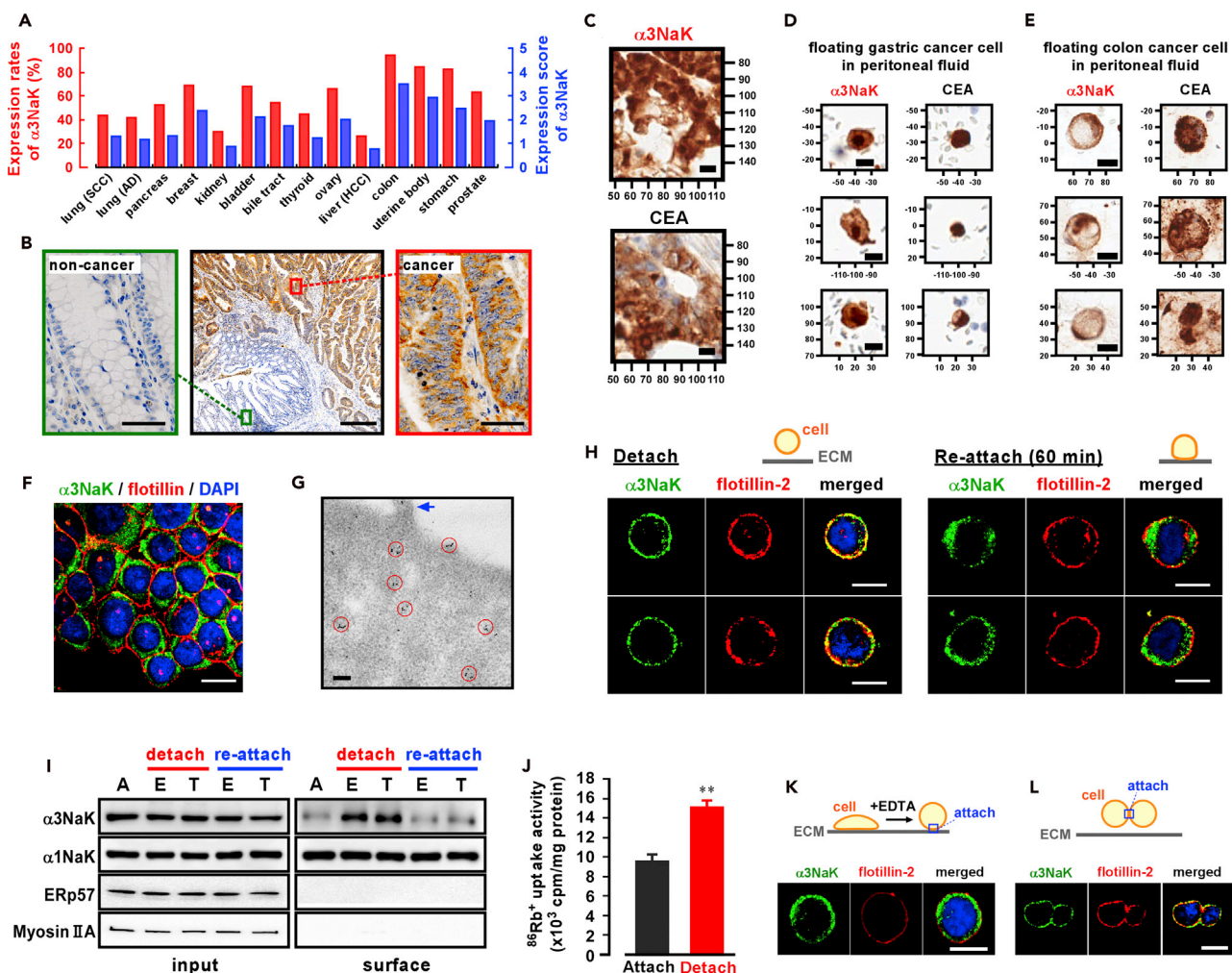


Figure 1. Translocation of $\alpha 3\text{NaK}$ to the PM by cell detachment

(A) Expression rates (left; red bars) and average expression scores (right; blue bars) of $\alpha 3\text{NaK}$ were assessed in tissue microarrays of multiple human cancers as shown in Figure S11.

(B) Immunohistochemistry of $\alpha 3\text{NaK}$ in human colorectal cancer tissue (patient No. 1, red frame) and adjacent noncancer mucosa (patient No. 1, green frame). Scale bars, 500 μm (middle panel) and 50 μm (left and right panels).

(C and D) Localization of $\alpha 3\text{NaK}$ in the cancer tissue (C) and floating cancer cells in the peritoneal fluid (D) from a patient with gastric cancer (patient No. 2). Cancer cells were identified by staining of CEA. Scale bars, 10 μm .

(E) Localization of $\alpha 3\text{NaK}$ in floating cancer cells in the peritoneal fluid of a patient with colon cancer (patient No. 3). Cancer cells were identified by staining of CEA. Scale bars, 10 μm .

(F) Fluorescent images of $\alpha 3\text{NaK}$ (green) and flotillin-2 (red) in attached HT-29 cells. Scale bar, 10 μm .

(G) An immunoelectron image of $\alpha 3\text{NaK}$ in attached HT-29 cells. Red circles indicate clusters of $\alpha 3\text{NaK}$ molecules underlying the PM. Blue arrow indicates a microvillus. Scale bar, 100 nm.

(H) Immunocytochemistry using antibodies for $\alpha 3\text{NaK}$ (green) and flotillin-2 (red) was performed in detached and re-attached HT-29 cells. Cells were detached by the treatment with the solution containing 0.25% trypsin and 10 mM EDTA. Scale bars, 10 μm .

(I) Surface biotinylation assay in HT-29 cells. Western blots of $\alpha 3\text{NaK}$, $\alpha 1\text{NaK}$, ERp57, and myosin IIA in the cell surface biotinylation samples (surface) and total cell lysates (input) of attached cells (A), detached cells (by 10 mM EDTA [E] or EDTA plus 0.25% trypsin [T]), and reattached cells.

(J) Ouabain (10 μM)-sensitive $^{86}\text{Rb}^+$ uptake activities of attached and detached HT-29 cells ($n = 7$). Cells were detached by treatment with the solution containing 10 mM EDTA. **, $p < 0.01$.

(K and L) Immunocytochemistry using antibodies for $\alpha 3\text{NaK}$ (green) and flotillin-2 (red) was performed in attached round-shaped cells which were attenuated their cell-matrix adhesion by treatment with 10 mM EDTA (K) and in detached doublet cells which keep their cell-cell adhesion (L). Scale bars, 10 μm .

congener. Cardiac glycoside (ouabain)-sensitive $^{86}\text{Rb}^+$ uptake activity in detached cells was significantly greater than in attached cells, suggesting that $\alpha 3\text{NaK}$ transferred from the cytoplasm to the PM is functional (Figures 1J and S11A). Furthermore, the localization of $\alpha 3\text{NaK}$ in the PM was also observed in single

cancer cells isolated from human colorectal cancer tissues by enzyme digestion (Figure S6). These results indicate that reversible translocation of $\alpha 3\text{NaK}$ between the PM and the cytoplasm is mediated by the cell detachment/attachment transition during the metastatic process of cancer cells.

Next, we examined whether the loss of cell-ECM attachment triggers the translocation of $\alpha 3\text{NaK}$ from the cytoplasm to the PM (PM translocation of $\alpha 3\text{NaK}$). Interestingly, the PM translocation of $\alpha 3\text{NaK}$ was not observed in round-shape attached cells that were partly but not completely have lost their cell-ECM adhesion (obtained by short-time treatment of EDTA; Figures 1K and S5C). In contrast, the PM translocation of $\alpha 3\text{NaK}$ occurred in the detached cell couplet in which cell-cell adhesion is still retained (Figures 1L and S5C). These results suggest that the loss of cell-ECM but not cell-cell adhesion is required for the $\alpha 3\text{NaK}$ translocation and that the change in cell curvature during the detachment process is not a trigger of the translocation.

Rab10, nicotinic acid adenine dinucleotide phosphate, and focal adhesion kinase are associated with the PM translocation of $\alpha 3\text{NaK}$

Because $\alpha 3\text{NaK}$ was colocalized with Rab10 in both attached and detached cancer cells (Figure S4), we assessed the effect of Rab10 knockdown on the PM translocation of $\alpha 3\text{NaK}$ in HT-29 cells. The total expression level of Rab10 was dramatically reduced in the Rab10-knockdown cells (Figure 2A). Interestingly, the surface expression level of $\alpha 3\text{NaK}$ was significantly decreased in the detached Rab10-knockdown cells, while the total expression level of $\alpha 3\text{NaK}$ was not changed (Figures 2B and 2C). Rab-GTPases-containing vesicle transport is mediated by actin filaments and microtubules (Hammer third and Wu, 2002). We then examined the effect of latrunculin B, an inhibitor of actin filament polymerization, on the detachment-induced PM translocation of $\alpha 3\text{NaK}$. As expected, latrunculin B significantly suppressed the expression level of $\alpha 3\text{NaK}$ but not $\alpha 1\text{NaK}$ in the PM of detached cells (Figures 2D, 2H, and S7). In addition, the PM translocation of $\alpha 3\text{NaK}$ but not $\alpha 1\text{NaK}$ was blocked when the cells were detached in cooled bathing solution ($\sim 4^\circ\text{C}$) (Figures 2E, 2H, and S7). These results suggest that the Rab10-related vesicular trafficking is involved in the PM translocation of $\alpha 3\text{NaK}$.

The Na^+, K^+ -ATPase β -subunit has essential roles in the trafficking and function of the α -subunit. To identify the β -subunit isoform for $\alpha 3\text{NaK}$ in human cancer cells, $\alpha 3\text{NaK}$ was immunoprecipitated using the anti- $\alpha 3\text{NaK}$ antibody in the lysate of HT-29 cells. Shotgun mass spectrometry with the elution fraction detected Na^+, K^+ -ATPase $\beta 1$ -isoform ($\beta 1\text{NaK}$) with high protein scores (Figure S8). In contrast, no scores of $\beta 2$ and $\beta 3$ isoforms were detected in the immunoprecipitation samples. Thus, $\alpha 3\text{NaK}$ may be coupled with $\beta 1\text{NaK}$ in the cells. Similarly, it has been reported that metastasized colorectal cancer cells express the $\alpha 3\text{NaK}$ - $\beta 1\text{NaK}$ complex and that the complex may potentially serve as a novel exploratory biomarker of colorectal cancer metastatic cells in the liver (Baker Bechmann et al., 2016).

We next examined the effects of Na^+, K^+ -ATPase inhibitors (cardiac glycosides; ouabain and oleandrin) on the detachment-induced PM translocation of $\alpha 3\text{NaK}$. Treatment of ouabain and oleandrin at $1 \mu\text{M}$ for 1 h significantly decreased the expression level of $\alpha 3\text{NaK}$ (but not $\alpha 1\text{NaK}$) in the PM of the detached cells (Figures 2E, 2H, and S7). In contrast, short-time treatment of ouabain (at $1 \mu\text{M}$ for 2 min) showed no significant change of the expression level of $\alpha 3\text{NaK}$ in the PM of the detached cells (Figures 2F and 2H). In the experiment to test the permeability of ouabain across the PM, uptake of [^3H]-ouabain into HT-29 cells was measured (Figure S9). The [^3H]-ouabain uptake was increased in a time-dependent and temperature-dependent manner and reached a maximum at 10 min (Figure S9). However, [^3H]-ouabain uptake was very low in 2-min treatment (Figure S9). These results suggest that function (activity) of intracellular $\alpha 3\text{NaK}$ may be important for the PM translocation of $\alpha 3\text{NaK}$.

Intracellular Ca^{2+} acts as a pivotal regulator of various cellular functions including vesicle trafficking and mechanotransduction (Brunger, 2001; Hay, 2007; Iqbal and Zaidi, 2005). Interestingly, we found that the detachment-induced PM translocation of $\alpha 3\text{NaK}$ was inhibited by Ca^{2+} -chelating agent BAPTA-AM and sarco/ER Ca^{2+} -ATPase (SERCA) inhibitors, thapsigargin, and cyclopiazonic acid (CPA) (Figures 2G and 2H). These compounds had no effects on the expression level of $\alpha 1\text{NaK}$ in the PM of the cells (Figure S7). Inositol 1,4,5-triphosphate (IP_3) and phospholipase C (PLC) are related to the Ca^{2+} release from ER through IP_3 receptor. However, the PM translocation of $\alpha 3\text{NaK}$ was not blocked by IP_3 receptor inhibitors, 2-aminoethoxydiphenyl borate (2-APB) and xestospongine, and a PLC inhibitor U73122 (Figures 2G and 2H). On the other hand, nicotinic acid adenine dinucleotide phosphate (NAADP) is one of the second messengers that release Ca^{2+} from

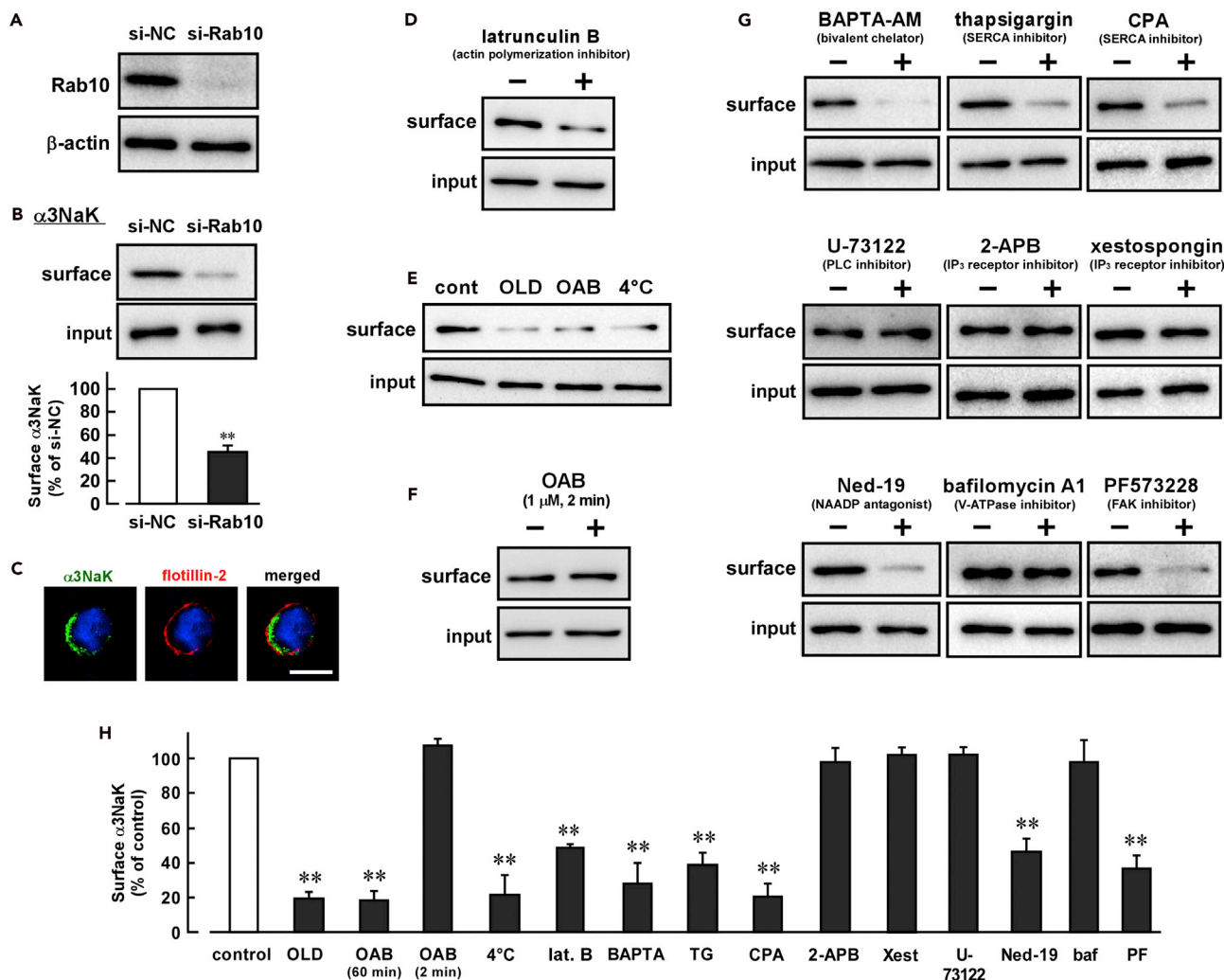


Figure 2. Detachment-induced α 3NaK translocation is mediated by Rab10, NAADP, and FAK

(A and B) Cell surface biotinylation in detached HT-29 cells transfected with Rab10 siRNA (si-Rab10) or negative control siRNA (si-NC). Western blots (WB) of Rab10 and α 3NaK in the total lysates (input) and biotinylation samples (surface). β -actin was used as a loading control. $n = 4$. **, $p < 0.01$.

(C) Immunocytochemistry using antibodies for α 3NaK (green) and flotillin-2 (red) was performed in detached Rab10-knockdown HT-29 cells. Scale bar, 10 μ m.

(D and E) Effect of latrunculin B (10 μ M, 1 h), oleandrin (OLD; 1 μ M, 1 h), ouabain (OAB; 1 μ M, 1 h), or cooled bath solution (\sim 4°C) on the surface expression level of α 3NaK in detached HT-29 cells.

(F) Effect of ouabain (1 μ M, 2 min) on the surface expression level of α 3NaK in detached cells.

(G) Effects of BAPTA-AM (100 μ M, 30 min), thapsigargin (10 μ M, 1 h), CPA (30 μ M, 1 h), U-73122 (5 μ M, 10 min), 2-APB (100 μ M, 1 hr), xestospingon C (4 μ M, 1 h), Ned-19 (100 μ M, 30 min), bafilomycin A1 (100 nM, 1 h), and PF573228 (500 nM, 1 h) on the surface expression level of α 3NaK in detached HT-29 cells.

(H) Quantification of the surface expression level of α 3NaK in D-G. $n = 4$ –5. **, $p < 0.01$. lat. B: latrunculin B; TG: thapsigargin; Xest: xestospingon C; baf: bafilomycin A1; PF: PF573228.

acidic stores such as the endosome and lysosome (Galione et al., 2011). Interestingly, NAADP antagonist Ned-19 (Naylor et al., 2009) that blocks NAADP-mediated Ca^{2+} signaling significantly reduced the PM translocation of α 3NaK in the cells (Figures 2G and 2H). Bafilomycin A1, an inhibitor of V-ATPase in the endosome and lysosome, had no effect on the translocation (Figures 2G and 2H). These results suggest that intracellular Ca^{2+} stores stimulated by NAADP but not IP_3 is involved in the PM translocation of α 3NaK translocation, whereas the endosome and lysosome are unlikely related to the mechanism.

Focal adhesion is a best-characterized cell-ECM adhesion structure (Worth and Parsons, 2008). Focal adhesion kinase (FAK) is a cytoplasmic tyrosine kinase localized at focal adhesions and plays a key function for integrin-mediated signal transductions (Sulzmaier et al., 2014). In the suspension culture of cancer cells,

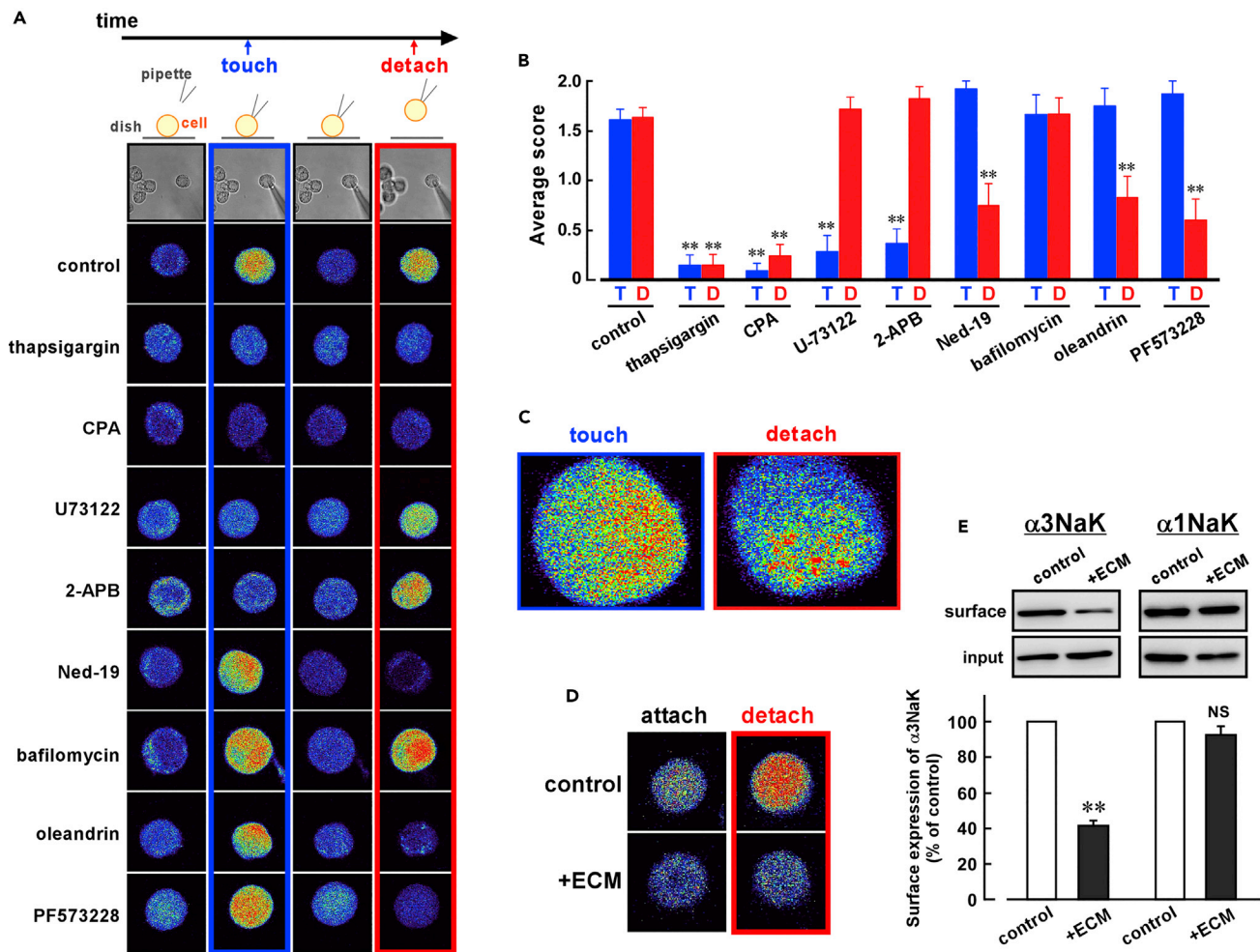


Figure 3. Unique $[\text{Ca}^{2+}]_i$ increase by detachment of cancer cells

(A) $[\text{Ca}^{2+}]_i$ imaging in HT-29 cells using Fluo-4. A cell was clamped (touch-stimulation) using a glass pipette in the Ca^{2+} -free solution. After the increase in $[\text{Ca}^{2+}]_i$, returned to basal level (~ 3 min), the cell was lifted (detach-stimulation). Effects of thapsigargin (10 μM , 1 h), CPA (30 μM , 1 h), U73122 (5 μM , 10 min), 2-APB (100 μM , 30 min), Ned-19 (100 μM , 30 min), bafilomycin A1 (100 nM, 1 h), oleandrin (1 μM , 30 min), and PF573228 (500 nM, 30 min) on the fluorescence of Fluo-4 under touch and detach stimulations.

(B) Fluo-4 fluorescence was scored as 0 (not significantly change), 1 (moderate increase), and 2 (marked increase) under touch or detach stimulations. $n = 46$ (control), $n = 11-18$ (drug treatments). **, $p < 0.01$ versus control.

(C) The region of $[\text{Ca}^{2+}]_i$ increase in the touch- and detach-stimulations was visualized.

(D) Effects of ECM solution (10 μM collagen and 10 μM fibronectin) on the fluorescence under touch and detach stimulations.

(E) Effects of ECM solution on the cell surface expression of $\alpha 3\text{NaK}$ and $\alpha 1\text{NaK}$ in the detached HT-29 cells. $n = 3$. **, $p < 0.01$; NS, $p > 0.05$.

activation of FAK is related to resistance to DICD (Kocí et al., 2011; Liu et al., 2008). Here, we found that PF573228, an inhibitor of FAK, significantly attenuated the expression level of $\alpha 3\text{NaK}$ in the PM of the detached HT-29 cells (Figures 2G and 2H). In contrast, it had no effect on the expression level of $\alpha 1\text{NaK}$ in the PM (Figure S7).

Cell detachment induces a unique Ca^{2+} response

To examine whether the detachment stimulus induces intracellular Ca^{2+} mobilization in cancer cells, the intracellular Ca^{2+} level ($[\text{Ca}^{2+}]_i$) in HT-29 cells was measured with a Ca^{2+} -sensitive dye Fluo-4. In the experiment under extracellular Ca^{2+} -free solution, the weakly attached cell on the dish was clamped (touch stimulation) and subsequently lifted (detach stimulation) using a glass pipette. As previously reported (Hansen et al., 1995; Moerenhout et al., 2001), transient increase in $[\text{Ca}^{2+}]_i$ was observed by the touch stimulation (Figures 3A and 3B). Interestingly, subsequent detach stimulation increased $[\text{Ca}^{2+}]_i$ again (Figures 3A and 3B). Given that these increases in $[\text{Ca}^{2+}]_i$ were observed in Ca^{2+} -free solution, the elevations after the touch or detach stimulation seemed to be

due to Ca^{2+} release from intracellular Ca^{2+} stores. Indeed, these $[\text{Ca}^{2+}]_i$ elevations were blocked by thapsigargin and CPA (Figures 3A and 3B). The $[\text{Ca}^{2+}]_i$ elevation by touch stimulation was significantly attenuated by 2-APB and U73122, whereas the detachment-induced $[\text{Ca}^{2+}]_i$ elevation was not (Figures 3A and 3B). In contrast, Ned-19 significantly inhibited only the detachment-induced $[\text{Ca}^{2+}]_i$ increase (Figures 3A and 3B). Bafilomycin A1 affected the $[\text{Ca}^{2+}]_i$ elevation by neither touch nor detach stimulation (Figures 3A and 3B). Notably, the region where $[\text{Ca}^{2+}]_i$ was elevated by detach stimulation was distinct from that by touch stimulation (Figure 3C). These results suggest that the touch stimulation triggers IP_3 -dependent Ca^{2+} release from the ER, whereas detachment-induced Ca^{2+} release mediated by NAADP is originated from the Ca^{2+} store other than the ER, endosome, and lysosome. In addition, oleandrin significantly attenuated the $[\text{Ca}^{2+}]_i$ increase by detach stimulation but not touch stimulation (Figures 3A and 3B), suggesting that function (activity) of $\alpha 3\text{NaK}$ may be involved in the Ca^{2+} response.

PF573228 (FAK inhibitor) significantly inhibited the detachment-induced $[\text{Ca}^{2+}]_i$ increase but not the touch-induced $[\text{Ca}^{2+}]_i$ increase (Figures 3A and 3B). Interestingly, the addition of ECM compounds (fibronectin and collagen) to the extracellular solution also inhibited the detachment-induced $[\text{Ca}^{2+}]_i$ increase and the PM translocation of $\alpha 3\text{NaK}$ but not of $\alpha 1\text{NaK}$ (Figures 3D and 3E). These results suggest that the Ca^{2+} response is mediated by the activation of FAK induced by loss of cell-ECM interaction.

SERCA3 is involved in the PM-translocation of $\alpha 3\text{NaK}$

SERCA pumps play a major role in the Ca^{2+} uptake into the intracellular Ca^{2+} stores. So far, three isoforms, SERCA1-3, have been identified. In the HT-29, HepG2, and MKN45 cells, expressions of SERCA2 and SERCA3 but not SERCA1 were observed (Figure 4A). SERCA3 was mainly colocalized with $\alpha 3\text{NaK}$ in the cytoplasm of the attached cells (Figure 4B), whereas SERCA2 was not (Figure S10). In the surface biotinylation assay, SERCA3 as well as $\alpha 3\text{NaK}$ was found to be translocated to the PM by cell detachment, while it was returned to the cytoplasm by the cell reattachment (Figure 4C). Knockdown of SERCA3 using the corresponding siRNA inhibited the detachment-induced $[\text{Ca}^{2+}]_i$ increase (Figure 4D) and the PM translocation of $\alpha 3\text{NaK}$ without affecting the total expression (input) level of $\alpha 3\text{NaK}$ (Figure 4E). On the other hand, both total and surface expression levels of $\alpha 1\text{NaK}$ were not significantly changed by the transfection of the SERCA3 siRNA (Figure 4E). These results suggest that the cell detachment elicits NAADP-dependent Ca^{2+} release from the SERCA3-expressing Ca^{2+} store.

FAK- and NAADP-dependent vesicle exocytosis is induced by cancer cell detachment

To examine whether intracellular vesicle is fused to the PM by the cancer cell detachment, we measured the membrane capacitance of HT-29 cells using whole-cell patch-clamp technique (Neher and Marty, 1982). Elevation of membrane capacitance corresponds to an enhancement of exocytosis (Kilic, 2002). In the attached cells, no significant change of membrane capacitance was observed (Figures 5A and 5G). Interestingly, the cell detachment significantly increased the membrane capacitance (Figures 5B and 5G), and the increase was disappeared under cold ($\sim 4^\circ\text{C}$) conditions (Figures 5C and 5G). In addition, Ned-19, PF573228, and oleandrin also significantly attenuated the detachment-increased membrane capacitance (Figures 5D–5G). These results suggest that FAK-dependent exocytosis of the $\alpha 3\text{NaK}$ -expressing vesicles may be elicited by the NAADP-dependent Ca^{2+} response upon cell detachment.

$\alpha 3\text{NaK}$ contributes to survival of the detached cancer cells

Metastatic cancer cells acquire resistance to DICD (Buchheit et al., 2012; Seyfried and Huysentruyt, 2013). To investigate whether the PM translocation of $\alpha 3\text{NaK}$ is required for the survival of the detached cancer cells, $\alpha 3\text{NaK}$ was knocked down by RNA interference (using $\alpha 3\text{NaK}$ -siRNA #1) in HT-29 cells. The expression level of $\alpha 3\text{NaK}$ was significantly decreased in $\alpha 3\text{NaK}$ -knockdown cells (Figure 6A). In fact, the increase in the ouabain-sensitive $^{86}\text{Rb}^+$ uptake activity upon detachment (Figure 1J) was inhibited in $\alpha 3\text{NaK}$ -knockdown cells (Figure S11A).

Interestingly, the silencing of $\alpha 3\text{NaK}$ significantly reduced the viability of the detached cells (assessed at 9 h after detachment) but not of the attached cells (Figure 6B). Transfection of another siRNA for $\alpha 3\text{NaK}$ ($\alpha 3\text{NaK}$ -siRNA #2) also decreased the expression level of $\alpha 3\text{NaK}$ and viability in detached cells (Figures S11B–S11D). In the $\alpha 3\text{NaK}$ -knockdown cells, the detachment-reduced viability was rescued by overexpression of cloned human $\alpha 3\text{NaK}$ (Figures 6A and 6B). On the other hand, knockdown of $\alpha 1\text{NaK}$ significantly decreased the viability of both attached cells and detached cells as expected (Figures S11E–S11G).

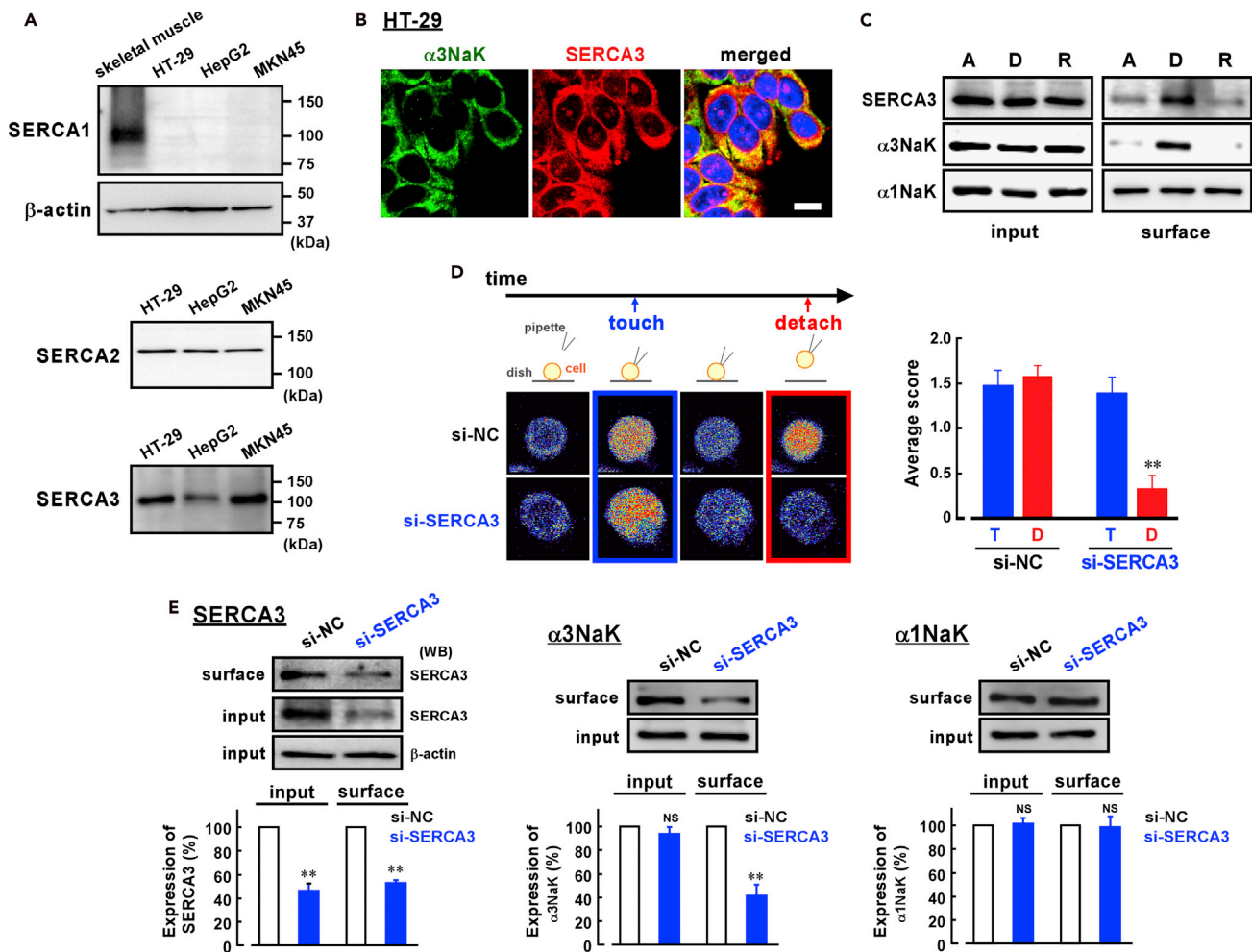


Figure 4. Involvement of SERCA3 in the detachment-induced events

(A) Expression of SERCA1, 2, and 3 in HT-29, HepG2, and MKN45 cells. As a positive control for SERCA1, human skeletal muscle was used. β -actin was used as a loading control.

(B) Immunocytochemistry using antibodies for α 3NaK and SERCA3 was performed in attached HT-29 cells. Scale bar, 10 μ m.

(C) Western blots of SERCA3, α 3NaK, and α 1NaK using the biotinylation samples (surface) and total lysates (input) of attached (A), detached (D), and re-attached (R) HT-29 cells. $n = 5$.

(D) Effect of the SERCA3 knockdown (si-SERCA3) on the $[Ca^{2+}]_i$ increase induced by touch and detach stimulations. As a control, cells transfected with negative control siRNA (si-NC) were examined. A cell was clamped (touch stimulation) using a glass pipette in the Ca^{2+} -free solution. After the increase in $[Ca^{2+}]_i$, returned to basal level (~ 3 min), the cell was lifted (detach-stimulation). $n = 19$. **, $p < 0.01$ vs si-NC.

(E) Western blots of SERCA3, α 3NaK, and α 1NaK using the biotinylation samples (surface) and total lysates (input) of detached HT-29 cells transfected with siRNA for SERCA3 (si-SERCA3) or si-NC. β -actin was used as a loading control. $n = 5$. **, $p < 0.01$; NS, $p > 0.05$.

Next, we examined the involvement of α 3NaK in the survival of the detached cancer cells using a heterologous expression system. The cloned human α 3NaK was overexpressed in mouse colorectal cancer colon 38 cells in which no significant expression of endogenous α 3NaK was observed (Figure 6C). Surface biotinylation assays suggested that the expression level of α 3NaK in the PM of detached cells was greater than the attached cells (Figure 6D). In immunocytochemistry, exogenous α 3NaK and endogenous Rab10 were found in the cytoplasm of the attached cells, whereas they were in the PM of the detached cells (Figure 6E). In the attached conditions, there is no significant difference in the cell viability between α 3NaK-transfected and empty-vector (mock)-transfected cells (Figure 6F). Interestingly, the viability of the α 3NaK-transfected cells was significantly greater than the mock-transfected cells in the detached conditions (assessed at 9 h after detachment) (Figure 6F). In the α 3NaK-transfected cells, the increased cell viability in a detached condition (Figure 6F) was significantly attenuated by treatment of Ned-19 (Figure S11H), suggesting the NAADP-dependent PM translocation of α 3NaK contributes to the cancer cell survival.

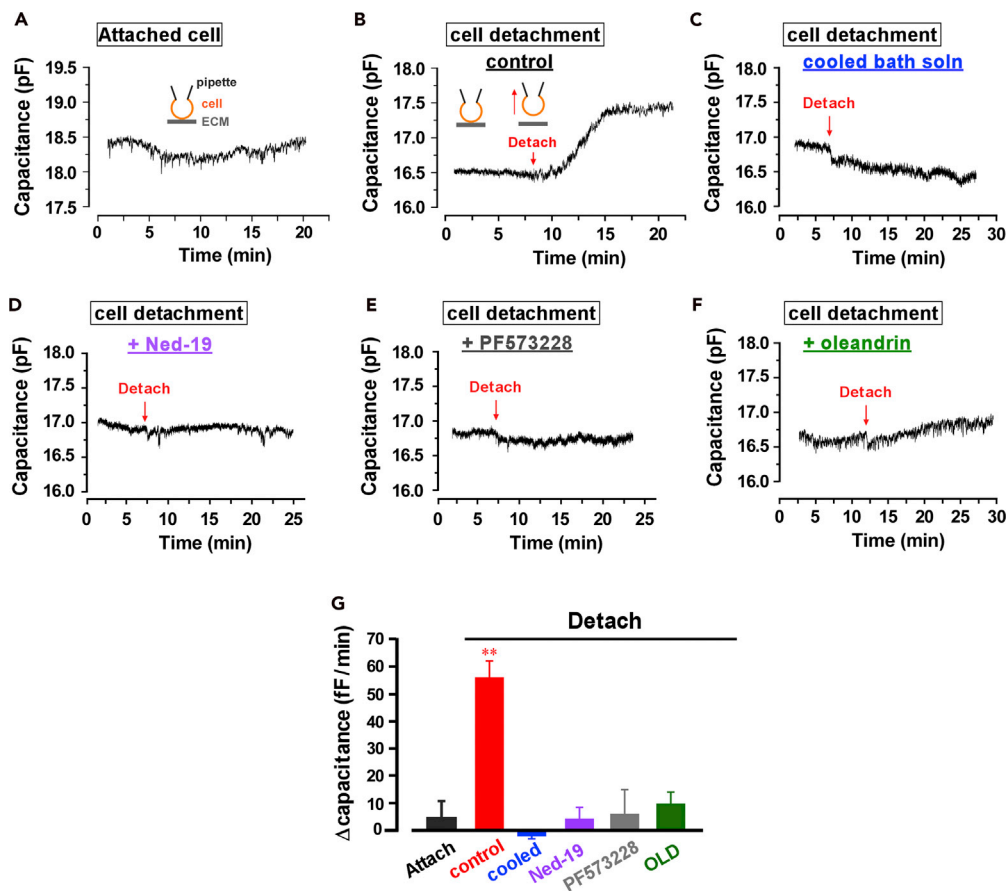


Figure 5. Increase in membrane capacitance upon cancer cell detachment

(A) Representative trace of membrane capacitance of attached HT-29 cells.

(B–F) The change in membrane capacitance by the cell detachment was measured. The control experiment is shown in (B). In (C), the cell was detached in a cooled bath solution. The cells were pre-treated with 100 μ M Ned-19 (D), 500 nM PF573228 (E), and 1 μ M oleandrin (F). Red arrows indicate the time point of the cell detachment. Representative traces were shown.

(G) The average rates of changes in membrane capacitance were shown. $n = 6-11$. **, $p < 0.01$.

We then measured the caspase 3/7 activity, which is activated during apoptosis in cancer cells. Silencing of $\alpha 3$ NaK further increased detachment-induced caspase 3/7 activation in HT-29 cells (assessed at 4 h after detachment; Figure 6G). Conversely, exogenous expression of $\alpha 3$ NaK significantly inhibited the detachment-induced caspase 3/7 activation in colon 38 cells (Figure 6H). These results suggest that the PM translocation of $\alpha 3$ NaK is responsible for the anchorage-independent survival of cancer cells.

To examine *in vivo* roles of $\alpha 3$ NaK in the detached cancer cells, the $\alpha 3$ NaK- or mock-transfected colon 38 cells were isolated from the culture dish. It was confirmed that no significant difference was observed between $\alpha 3$ NaK- and mock-transfected colon 38 cells at 20 min after detachment ($95.3\% \pm 1.1\%$ and $93.5\% \pm 2.1\%$, respectively), and the cells were subcutaneously injected into mice within 15 min. Subcutaneous tumors were isolated from the mice and measured their wet weights at 5 and 10 days after injection. The weight of the tumor obtained from $\alpha 3$ NaK-overexpressing cells was significantly greater than that from mock-transfected cells (Figure 7A). The mRNA of exogenous human $\alpha 3$ NaK was detected in the isolated tumor tissues (Figure S12).

To identify the association of $\alpha 3$ NaK with metastasis *in vivo*, $\alpha 3$ NaK- and mock-transfected colon 38 cells were injected into the tail vein of mice. In a control experiment, mRNA expression derived from the transfected vector (pcDNA4) in the colon 38 cells was measured by the quantitative real-time polymerase chain reaction (PCR) analysis. No significant difference in transfection efficiency was observed between the

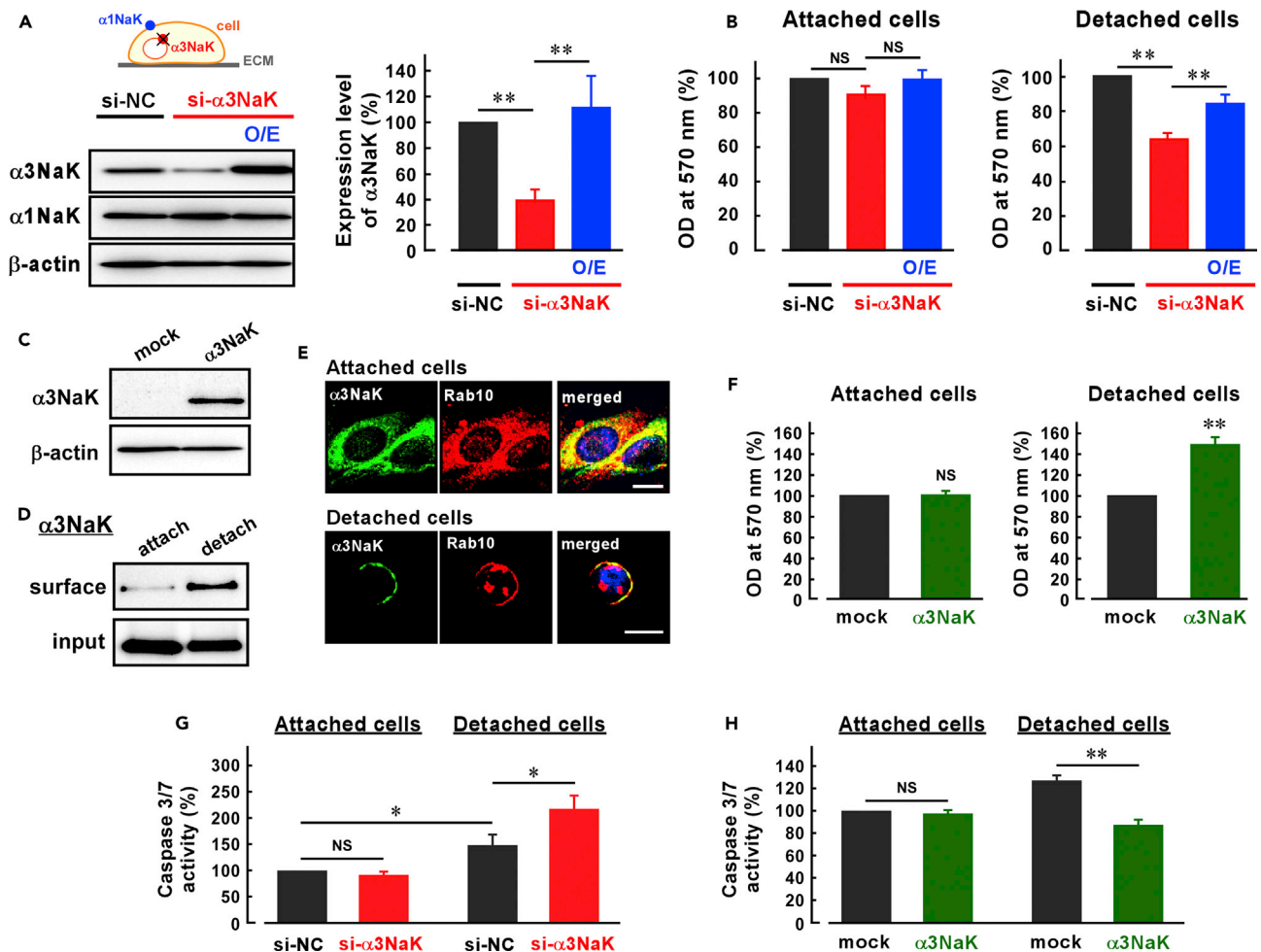


Figure 6. α 3NaK is involved in survival of the detached cancer cells

(A) Western blots in HT-29 cells transfected with α 3NaK-siRNA (#1) (si- α 3NaK), α 3NaK-siRNA (#1) (si- α 3NaK) plus α 3NaK-expression vector (O/E), or negative control siRNA (si-NC). The expression level of α 3NaK was normalized to that of β -actin (n = 7). **, p < 0.01.

(B) Cell viability of attached and detached HT-29 cells. The viability in α 3NaK-siRNA (#1)-transfected cells was compared with α 3NaK-siRNA (#1) plus α 3NaK-expression vector (O/E)-transfected cells and si-NC-transfected cells (n = 7). **, p < 0.01. NS, p > 0.05.

(C) Expression of α 3NaK in the human α 3NaK-transfected and the empty vector-transfected (mock) colon 38 cells. β -actin was used as a loading control.

(D) Western blots in cell surface biotinylation samples (surface) and total lysates (input) of attached and detached α 3NaK-transfected colon 38 cells.

(E) Immunocytochemistry of α 3NaK and Rab10 in attached and detached α 3NaK-transfected colon 38 cells. Scale bars, 10 μ m.

(F) Effect of exogenous α 3NaK expression on cell viability. Attached and detached colon 38 cells were used. The viability in α 3NaK-transfected cells was compared with mock-transfected cells (n = 5). **, p < 0.01. NS, p > 0.05.

(G) Effect of α 3NaK knock down on caspase 3/7 activity. Attached and detached HT-29 cells were used. The activity in α 3NaK-siRNA-transfected cells (si- α 3NaK) was compared with NC-siRNA-transfected cells (si-NC) (n = 5–7). *, p < 0.05. NS, p > 0.05.

(H) Effect of exogenous α 3NaK expression on caspase 3/7 activity. Attached and detached colon 38 cells were used. The activity in α 3NaK-transfected cells was compared with mock-transfected cells (n = 6). **, p < 0.01. NS, p > 0.05.

α 3NaK- and mock-transfected cells (Figure 7B). Seven days after injection, the lung was removed and total RNA was prepared. Metastasis of cancer cells in the lung was evaluated by quantitative real-time PCR analysis. The amount of the vector (corresponding to the number of the colon 38 cells) in the lungs of mice injected with α 3NaK-transfected cells was significantly higher than those injected with mock-transfected cells (Figure 7C). These results suggest that α 3NaK contributes to the survival of the detached cancer cells *in vivo*.

Activation of AMPK is involved in downstream of the PM translocation of α 3NaK

How does α 3NaK confer survival signaling in the detached cancer cells? Here, we focused on AMPK and reactive oxygen species (ROS). AMPK has been known to have an essential role in anoikis resistance.

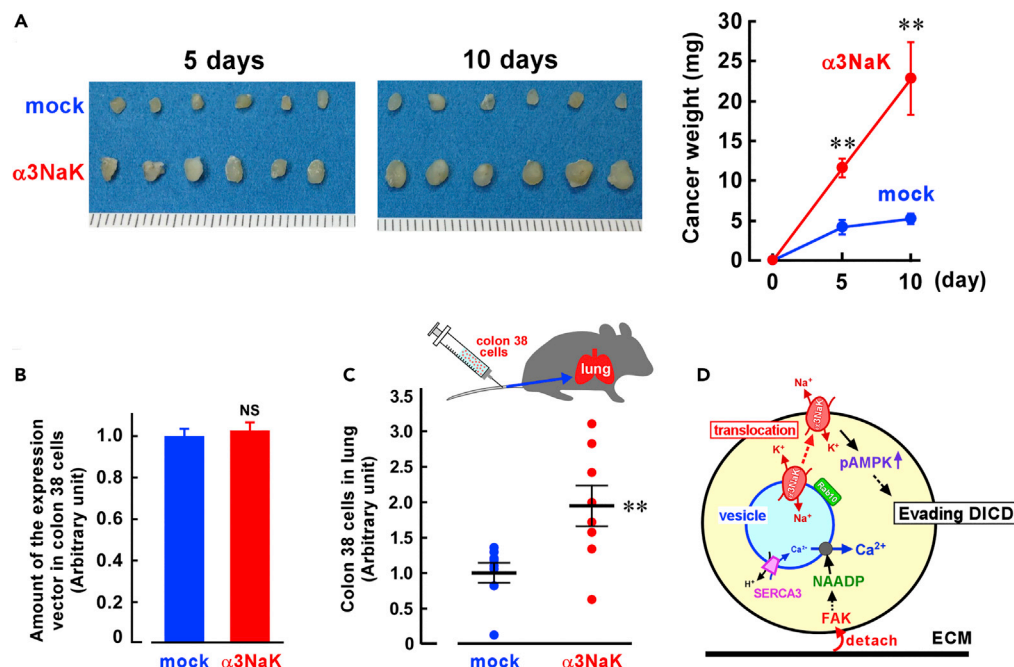


Figure 7. Expression of $\alpha 3\text{NaK}$ promotes tumor growth and metastasis *in vivo*

(A) $\alpha 3\text{NaK}$ - and mock-transfected colon 38 cells were subcutaneously implanted into the flank of mice. Five and 10 days after injection, cancer tissues were dissected, photographed, and weighed. Three independent experiments were conducted with six mice for each group. **, $p < 0.01$.

(B) Relative mRNA expression levels derived from the pcDNA4 vector in the $\alpha 3\text{NaK}$ - and mock-transfected colon 38 cells were assessed by quantitative real-time PCR analysis. ($n = 4$). NS, $p > 0.05$.

(C) $\alpha 3\text{NaK}$ - and mock-transfected colon 38 cells were injected into the tail vein of mice. Seven days after injection, lung was removed and total RNA was prepared. Relative mRNA expression levels derived from the pcDNA4 vector (corresponding to the number of the colon 38 cells) in the lungs were assessed by quantitative real-time PCR analysis. ($n = 8$). **, $p < 0.01$.

(D) The proposed model of the detachment-induced events in cancer cells.

AMPK is phosphorylated at position 172 (threonine residue) and activated upon matrix deprivation (Sundararaman et al., 2016; Jin et al., 2018). We then examined the association between $\alpha 3\text{NaK}$ and AMPK in detached cancer cells (Figure 8A). As previous reports, cell detachment activated the phosphorylation of AMPK at threonine 172 in HT-29 cells. Interestingly, knockdown of $\alpha 3\text{NaK}$ suppressed the detachment-induced phosphorylation of AMPK (Figure 8A). These results suggest that activation of AMPK is associated with the translocated $\alpha 3\text{NaK}$ for survival of detached cancer cells. On the other hand, increase in intracellular Ca^{2+} and ROS has been reported to be involved in the AMPK phosphorylation (Sundararaman et al., 2016). However, no significant difference in the ROS level was observed in the $\alpha 3\text{NaK}$ -knockdown cells upon cell detachment (Figure 8B).

DISCUSSION

In this study, we found that $\alpha 3\text{NaK}$ in intracellular vesicles are dynamically translocated to the PM by loss of anchorage in the cancer cells and that this mechanism is mediated by FAK- and NAADP-dependent Ca^{2+} mobilization (Figure 7D). Patch-clamp capacitance measurements also demonstrated the induction of the vesicle exocytosis by the FAK- and NAADP-dependent pathway upon cancer cell detachment. The expression of $\alpha 3\text{NaK}$ in the PM was detected in floating cancer cells obtained from peritoneal fluids of patients. Our *in vitro* and *in vivo* studies showed that the PM-translocation of $\alpha 3\text{NaK}$ contributes to the survival of the detached cancer cells.

$\alpha 3\text{NaK}$ has been thought to be predominantly expressed in the PM of the neuronal cells. However, our tissue microarray analysis showed that the expression of $\alpha 3\text{NaK}$ was widely observed in the cytoplasm of various types of human cancer cells. In the cells, $\alpha 3\text{NaK}$ was colocalized with Rab10 which is a key regulator

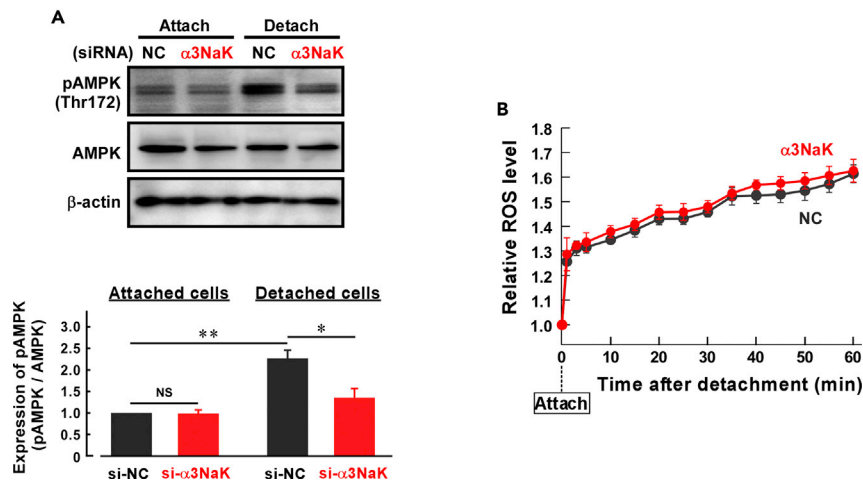


Figure 8. Downstream of the PM-translocation of $\alpha 3\text{NaK}$

(A) Effect of $\alpha 3\text{NaK}$ -knockdown on the AMPK phosphorylation. Expression of pAMPK (Thr172), total AMPK, and β -actin in attached and detached HT-29 cells transfected with siRNA for $\alpha 3\text{NaK}$ (#1) ($\alpha 3\text{NaK}$) or NC-siRNA (NC). The expression level of pAMPK (Thr172) was normalized to that of total AMPK ($n = 3$). * $p < 0.05$; ** $p < 0.01$; NS, $p > 0.05$.

(B) Effect of $\alpha 3\text{NaK}$ -knockdown on the intracellular ROS generation. Intracellular ROS level in HT-29 cells transfected with siRNA for $\alpha 3\text{NaK}$ (#1) ($\alpha 3\text{NaK}$) or NC-siRNA (NC). Cells were treated with EDTA for 5 min and were detached by gently pipetting. The fluorescence was sequentially measured from 0 min (attached cells; before pipetting) to 60 min ($n = 4$).

of intracellular vesicle trafficking (Stenmark, 2009). Here, the knockdown of Rab10 significantly inhibited the detachment-induced translocation of $\alpha 3\text{NaK}$ in the cancer cells. In addition, we found that $\alpha 3\text{NaK}$ is colocalized with SERCA3 in the cells. SERCA Ca^{2+} pumps are generally involved in maintaining and replenishing internal Ca^{2+} stores. The knockdown of SERCA3 inhibited the detachment-induced Ca^{2+} mobilization and the PM translocation of $\alpha 3\text{NaK}$. Cardiac glycoside (oleandrin) inhibited the detachment-induced Ca^{2+} mobilization and subsequent vesicle exocytosis. These results suggest that the vesicles which express $\alpha 3\text{NaK}$, Rab10, and SERCA3 can function as a Ca^{2+} store for the detachment-induced Ca^{2+} release (Figure 6H). Interestingly, the Ca^{2+} release was suppressed by inhibitors of NAADP and FAK but not of IP_3R , PLC, and V-ATPase. To our knowledge, such Ca^{2+} store with a unique pharmacological property has not been reported to date. Rab10 was highly expressed in human liver cancer tissues (He et al., 2002; Wang et al., 2017), and the Rab10 overexpression in the cancer tissues correlated with poor prognosis including distant metastasis (Wang et al., 2017). Our results suggest that Rab10 may regulate translocation of the $\alpha 3\text{NaK}$ and SERCA3-expressing vesicles, resulting in cancer cell malignancy. Furthermore, our proteome analysis indicated $\alpha 3\text{NaK}$ is coupled with $\beta 1\text{NaK}$ (not $\beta 2\text{NaK}$ and $\beta 3\text{NaK}$) in the intracellular Rab10-expressing vesicles of HT-29 cells. β -subunit plays a crucial role for the trafficking and functional expression of α -subunit of Na^+, K^+ -ATPase including $\alpha 3\text{NaK}$ (Dobretsov and Stimers, 2005). Interestingly, $\alpha 3\text{NaK}$ is also associated with $\beta 1\text{NaK}$ in PM of neuronal cells (Shrivastava et al., 2015). Future studies are needed to clarify why the $\alpha 3\text{NaK}$ - $\beta 1\text{NaK}$ complex is localized in the intracellular vesicles rather than PM of the attached cancer cells. In addition, detachment-induced vesicle exocytosis and PM translocation of $\alpha 3\text{NaK}$ were significantly inhibited by oleandrin, suggesting that function of the $\alpha 3\text{NaK}$ - $\beta 1\text{NaK}$ complex may play an important role in the translocation.

It has recently been reported that the administration of cardiac glycosides (ouabain and digoxin) remarkably reduced the total metastatic burden in *in vivo* mouse models (Gkountela et al., 2019): Inhibition of Na^+, K^+ -ATPase leads to increase in $[\text{Ca}^{2+}]_i$, resulting in dissociation of circulating tumor cells (CTCs) clusters which is associated with the increased metastatic potential. In addition, ouabain targets $\alpha 3\text{NaK}$ to inhibit cell proliferation and induce apoptosis in human OS-RC-2 renal cancer cells and human NCI-H446 small-cell lung cancer cells (Xiao et al., 2017). Bufalin, a cardiac glycoside, induced apoptosis of human T24 bladder carcinoma cells through inactivation of $\alpha 3\text{NaK}$ (Huang and Zhang, 2018). In the present study, the knockdown and overexpression of $\alpha 3\text{NaK}$ demonstrate that the PM translocation of $\alpha 3\text{NaK}$ is involved in the survival of the detached cancer cells, whereas $\alpha 1\text{NaK}$ unlikely contributes to this mechanism. The ouabain-sensitive $^{86}\text{Rb}^+$ -uptake activity of cancer cells was increased upon cancer cell detachment,

suggesting functional expression of $\alpha 3$ NaK in the PM. The contribution of $\alpha 3$ NaK function in the PM to the formation of the CTCs clustering remains to be elucidated in a future study.

Disassembly of focal adhesions is necessary to cellular migration and FAK is associated with this process (McLean et al., 2005). FAK is normally activated when the cells attach to appropriate matrix proteins. However, it is noted that FAK is activated in human epidermal cancer cells under the detached culture conditions and that the FAK activation could stimulate tumor cell migration and therefore induce metastasis (Kabayama et al., 2008). In addition, the administration of an NAADP antagonist Ned-19 strongly reduced the number of lung metastases of B16 melanoma cells in *in vivo* studies and FAK inactivation is involved in the mechanism (Favia et al., 2016). Thus, the FAK-NAADP axis is thought to be involved in metastasis mechanisms. Here, we found that both Ned-19 and FAK inhibitors significantly block the detachment-induced $[Ca^{2+}]_i$ increase and the PM translocation of $\alpha 3$ NaK, suggesting the involvement of FAK and NAADP in a unique Ca^{2+} response induced by cancer cell detachment. In fact, Ca^{2+} signals are elicited by external forces such as stretching tension, scratch, compression, shear force, and osmotic pressure. FAK is one of the molecules related to cell-ECM contacts and functions as a mechanosensor translating the force into biochemical signals (Hytönen and Wehrle-Haller, 2016). Therefore, our study may be the first report describing mechanosensing machinery induced by loss of cell-ECM anchorage.

We also found that phosphorylation of AMPK is stimulated in the detached cancer cells and that silencing of $\alpha 3$ NaK suppresses the detachment-induced phosphorylation of AMPK. In contrast, no significant difference was observed in intracellular ROS levels in the $\alpha 3$ NaK-knockdown cells. These results suggest that activation of AMPK is involved in downstream of the PM translocation of $\alpha 3$ NaK. Mechanism of functional relationship between $\alpha 3$ NaK and AMPK in the anoikis resistance is an important topic for future research.

In conclusion, we revealed a novel mechanotransduction upon cell-ECM detachment which gives rise to a dynamic translocation of $\alpha 3$ NaK to the PM for metastatic cancer cell survival. Therefore, $\alpha 3$ NaK may be a potent therapeutic target for inhibiting metastasis of cancer cells.

Limitations of the study

Our *in vivo* and *in vitro* analysis demonstrated that NAADP-dependent Ca^{2+} -signaling-induced translocation of $\alpha 3$ NaK to the PM is involved in cell survival of detached cancer cells. We also showed that the PM translocation of $\alpha 3$ NaK was observed in the floating cancer cells in the peritoneal fluid of patients with gastric and colon cancer and the single cancer cells isolated from human colorectal cancer tissues by enzyme digestion. However, the intracellular phenomenon at the moment when cancer cells spontaneously detach from the primary tissue has not been verified for technical and ethical reasons. Furthermore, to expand our findings, it is important to investigate the localization and function of $\alpha 3$ NaK in CTCs isolated from patients with cancer.

Resource availability

Lead contact

Further information and requests for resources and reagents should be directed to and will be fulfilled by the Lead Contact, Hideki Sakai (sakaih@pha.u-toyama.ac.jp).

Materials availability

This work did not generate new unique reagents.

Data and code availability

This article includes all analyzed data.

METHODS

All methods can be found in the accompanying [transparent methods supplemental file](#).

SUPPLEMENTAL INFORMATION

Supplemental information can be found online at <https://doi.org/10.1016/j.isci.2021.102412>.

ACKNOWLEDGMENTS

This article is dedicated to the memory of Prof. Kazuhiro Tsukada, who provided tremendous supports and conceptual advice. He passed away in March 2016. We thank T. Watanabe for support for providing clinical samples. E. Shimoda, A. Honryo, K. Funayama, A. Fujitsugu, T. Horaguchi, and S. Yamamoto for technical assistance. A. Ito for technical support with mouse model. This work was supported in part by Grants-in-Aid for Scientific Research (KAKENHI) from the Japan Society for the Promotion of Science and the Ministry of Education, Culture, Sports, Science and Technology of Japan (to Ta.F. (JP26460291, JP17K08531, and JP20K07258), T.S. (JP16K08490), and H.S. (JP15K15029)), Tamura Science & Technology Foundation, Platform for drug discovery, informatics and structural life science, and Academic drug discovery support project commissioned by Toyama Prefecture.

AUTHORS CONTRIBUTION

Ta.F. and H.S. designed all experiments. Ta.F., T.S. M.K, and Y.T. performed *in vitro* and *in vivo* studies. S.N. performed proteome analysis. K.S., T.O., and Ts.F provided clinical samples. J.F. performed histological studies and analyzed data. K.K. supported *in vivo* studies. A.S. performed immunoelectron microscopic analysis. H.T. gave conceptual advice. Ta.F. and H.S. wrote the manuscript with assistance from other authors.

DECLARATION OF INTERESTS

The authors declare that there are no conflicts of interest.

Received: September 16, 2020

Revised: February 28, 2021

Accepted: April 6, 2021

Published: May 21, 2021

REFERENCES

- Baker Bechmann, M., Rotoli, D., Morales, M., Maeso, M., García, M., Ávila, J., Mobasheri, A., and Martín-Vasallo, P. (2016). Na,K-ATPase Isozymes in colorectal cancer and liver metastases. *Front. Physiol.* 7, 9.
- Brunner, A.T. (2001). Structural insights into the molecular mechanism of calcium-dependent vesicle-membrane fusion. *Curr. Opin. Struct. Biol.* 11, 163–173.
- Buchheit, C.L., Rayavarapu, R.R., and Schafer, Z.T. (2012). The regulation of cancer cell death and metabolism by extracellular matrix attachment. *Semin. Cell Dev. Biol.* 23, 402–411.
- Calderón-Montaño, J.M., Burgos-Morón, E., Orta, M.L., Maldonado-Navas, D., García-Domínguez, I., and López-Lázaro, M. (2014). Evaluating the cancer therapeutic potential of cardiac glycosides. *Biomed. Res. Int.* 2014, 794930.
- Diederich, M., Müller, F., and Cerella, C. (2017). Cardiac glycosides: from molecular targets to immunogenic cell death. *Biochem. Pharmacol.* 125, 1–11.
- Dobretsov, M., and Stimers, J.R. (2005). Neuronal function and alpha3 isoform of the Na/K-ATPase. *Front. Biosci.* 10, 2373–2396.
- Durlacher, C.T., Chow, K., Chen, X.-W., He, Z.-X., Zhang, X., Yang, T., and Zhou, S.-F. (2015). Targeting Na⁺/K⁺-translocating adenosine triphosphatase in cancer treatment. *Clin. Exp. Pharmacol. Physiol.* 42, 427–443.
- Favia, A., Pafumi, I., Desideri, M., Padula, F., Montesano, C., Passeri, D., Nicoletti, C., Orlandi, A., Del Bufalo, D., Sergi, M., et al. (2016). NAADP-dependent Ca²⁺ signaling controls melanoma progression, metastatic dissemination and neoangiogenesis. *Sci. Rep.* 6, 18925.
- Fujii, T., Shimizu, T., Yamamoto, S., Funayama, K., Fujita, K., Tabuchi, Y., Ikari, A., Takeshima, H., and Sakai, H. (2018). Crosstalk between Na⁺/K⁺-ATPase and a volume-regulated anion channel in membrane microdomains of human cancer cells. *Biochim. Biophys. Acta Mol. Basis Dis.* 1864, 3792–3804.
- Galione, A., Parrington, J., and Funnell, T. (2011). Physiological roles of NAADP-mediated Ca²⁺ signaling. *Sci. China Life Sci.* 54, 725–732.
- Gkoutela, S., Castro-Giner, F., Szczerba, B.M., Vetter, M., Landin, J., Scherrer, R., Krol, I., Scheidmann, M.C., Beisel, C., Stirnimann, C.U., et al. (2019). Circulating tumor cell clustering shapes DNA methylation to enable metastasis seeding. *Cell* 176, 98–112.
- Guadamillas, M.C., Cerezo, A., and Del Pozo, M.A. (2011). Overcoming anoikis—pathways to anchorage-independent growth in cancer. *J. Cell Sci.* 124, 3189–3197.
- Hansen, M., Boitano, S., Dirksen, E.R., and Sanderson, M.J. (1995). A role for phospholipase C activity but not ryanodine receptors in the initiation and propagation of intercellular calcium waves. *J. Cell Sci.* 108, 2583–2590.
- Hay, J.C. (2007). Calcium: a fundamental regulator of intracellular membrane fusion? *EMBO Rep.* 8, 236–240.
- He, H., Dai, F., Yu, L., She, X., Zhao, Y., Jiang, J., Chen, X., and Zhao, S. (2002). Identification and characterization of nine novel human small GTPases showing variable expressions in liver cancer tissues. *Gene Expr.* 10, 231–242.
- Holm, T.H., and Lykke-Hartmann, K. (2016). Insights into the pathology of the $\alpha 3$ Na⁺/K⁺-ATPase ion pump in neurological disorders; Lessons from animal models. *Front. Physiol.* 7, 209.
- Huang, H., and Zhang, W. (2018). Bufalin induced apoptosis of bladder carcinoma cells through the inactivation of Na⁺+K⁺-ATPase. *Oncol. Lett.* 16, 3826–3832.
- Hytönen, V.P., and Wehrle-Haller, B. (2016). Mechanosensing in cell-matrix adhesions - converting tension into chemical signals. *Exp. Cell Res.* 343, 35–41.
- Iqbal, J., and Zaidi, M. (2005). Molecular regulation of mechanotransduction. *Biochem. Biophys. Res. Commun.* 328, 751–755.
- Jin, L., Chun, J., Pan, C., Kumar, A., Zhang, G., Ha, Y., Li, D., Alesi, G.N., Kang, Y., Zhou, L., et al. (2018). The PLAG1-GDH1 axis promotes anoikis resistance and tumor metastasis through CamKK2-AMPK signaling in LKB1-deficient lung cancer. *Mol. Cell* 69, 87–99.
- Katayama, H., Yamane, Y., Furukawa, Y., Kitagawa, S., Nakamura, Y., and Yoshino, K.

- (2008). Activation of focal adhesion kinase in detached human epidermal cancer cells and their long-term survival might be associated with cell surface expression of laminin-5. *Acta Derm. Venereol.* **88**, 100–107.
- Kilic, G. (2002). Exocytosis in bovine chromaffin cells: studies with patch-clamp capacitance and FM1-43 fluorescence. *Biophys. J.* **83**, 849–857.
- Kočí, L., Hýžd'álová, M., Vaculová, A., Hofmanová, J., and Kozubík, A. (2011). Detachment-mediated resistance to TRAIL-induced apoptosis is associated with stimulation of the PI3K/Akt pathway in fetal and adenocarcinoma epithelial colon cells. *Cytokine* **55**, 34–39.
- Liu, G., Meng, X., Jin, Y., Bai, J., Zhao, Y., Cui, X., Chen, F., and Fu, S. (2008). Inhibitory role of focal adhesion kinase on anoikis in the lung cancer cell A549. *Cell Biol. Int.* **32**, 663–670.
- McLean, G.W., Carragher, N.O., Avizienyte, E., Evans, J., Brunton, V.G., and Frame, M.C. (2005). The role of focal-adhesion kinase in cancer—a new therapeutic opportunity. *Nat. Rev. Cancer* **5**, 505–515.
- Moerenhout, M., Vereecke, J., and Himpens, B. (2001). Mechanism of intracellular Ca^{2+} -wave propagation elicited by mechanical stimulation in cultured endothelial CPAE cells. *Cell Calcium* **29**, 117–123.
- Naylor, E., Arredouani, A., Vasudevan, S.R., Lewis, A.M., Parkesh, R., Mizote, A., Rosen, D., Thomas, J.M., Izumi, M., Ganesan, A., et al. (2009). Identification of a chemical probe for NAADP by virtual screening. *Nat. Chem. Biol.* **5**, 220–226.
- Neher, E., and Marty, A. (1982). Discrete changes of cell membrane capacitance observed under conditions of enhanced secretion in bovine adrenal chromaffin cells. *Proc. Natl. Acad. Sci. U S A* **79**, 6712–6716.
- Sakai, H., Suzuki, T., Maeda, M., Takahashi, Y., Horikawa, N., Minamimura, T., Tsukada, K., and Takeguchi, N. (2004). Up-regulation of Na^+ , K^+ -ATPase α 3-isoform and down-regulation of the α 1-isoform in human colorectal cancer. *FEBS Lett.* **563**, 151–154.
- Seyfried, T.N., and Huysentruyt, L.C. (2013). On the origin of cancer metastasis. *Crit. Rev. Oncog.* **18**, 43–73.
- Shibuya, K., Fukuoka, J., Fujii, T., Shimoda, E., Shimizu, T., Sakai, H., and Tsukada, K. (2010). Increase in ouabain-sensitive K^+ -ATPase activity in hepatocellular carcinoma by overexpression of Na^+ , K^+ -ATPase α 3-isoform. *Eur. J. Pharmacol.* **638**, 42–46.
- Shrivastava, A.N., Redeker, V., Fritz, N., Pieri, L., Almeida, L.G., Spolidoro, M., Liebmann, T., Bousset, L., Renner, M., Léna, C., et al. (2015). α -synuclein assemblies sequester neuronal α 3- Na^+ / K^+ -ATPase and impair Na^+ gradient. *EMBO J.* **34**, 2408–2423.
- Stenmark, H. (2009). Rab GTPases as coordinators of vesicle traffic. *Nat. Rev. Mol. Cell Biol.* **10**, 513–525.
- Sulzmaier, F.J., Jean, C., and Schlaepfer, D.D. (2014). FAK in cancer: mechanistic findings and clinical applications. *Nat. Rev. Cancer* **14**, 598–610.
- Sundararaman, A., Amirtham, U., and Rangarajan, A. (2016). Calcium-oxidant signaling network regulates AMP-activated protein kinase (AMPK) activation upon matrix deprivation. *J. Biol. Chem.* **291**, 14410–14429.
- Wang, W., Jia, W.D., Hu, B., and Pan, Y.Y. (2017). RAB10 overexpression promotes tumor growth and indicates poor prognosis of hepatocellular carcinoma. *Oncotarget* **8**, 26434–26447.
- Worth, D.C., and Parsons, M. (2008). Adhesion dynamics: mechanisms and measurements. *Int. J. Biochem. Cell Biol.* **40**, 2397–2409.
- Hammer, J.A., 3rd, and Wu, X.S. (2002). Rabs grab motors: defining the connections between Rab GTPases and motor proteins. *Curr. Opin. Cell Biol.* **14**, 69–75.
- Xiao, Y., Meng, C., Lin, J., Huang, C., Zhang, X., Long, Y., Huang, Y., and Lin, Y. (2017). Ouabain targets the Na^+ / K^+ -ATPase α 3 isoform to inhibit cancer cell proliferation and induce apoptosis. *Oncol. Lett.* **14**, 6678–6684.
- Yang, P., Menter, D.G., Cartwright, C., Chan, D., Dixon, S., Suraokar, M., Mendoza, G., Llansa, N., and Newman, R.A. (2009). Oleandrin-mediated inhibition of human tumor cell proliferation: importance of Na, K -ATPase alpha subunits as drug targets. *Mol. Cancer Ther.* **8**, 2319–2328.
- Yang, P., Cartwright, C., Efuot, E., Hamilton, S.R., Wistuba, I.I., Menter, D., Addington, C., Shureiqi, I., and Newman, R.A. (2014). Cellular location and expression of Na^+ , K^+ -ATPase α subunits affect the anti-proliferative activity of oleandrin. *Mol. Carcinog.* **53**, 253–263.
- Yawata, A., Adachi, M., Okuda, H., Naishiro, Y., Takamura, T., Hareyama, M., Takayama, S., Reed, J.C., and Imai, K. (1998). Prolonged cell survival enhances peritoneal dissemination of gastric cancer cells. *Oncogene* **16**, 2681–2686.

Supplemental information

Survival of detached cancer cells is regulated by movement of intracellular Na^+, K^+ -ATPase

Takuto Fujii, Takahiro Shimizu, Mizuki Katoh, Shushi Nagamori, Keiichi Koizumi, Junya Fukuoka, Yoshiaki Tabuchi, Akira Sawaguchi, Tomoyuki Okumura, Kazuto Shibuya, Tsutomu Fujii, Hiroshi Takeshima, and Hideki Sakai

Supplemental Information

Supplemental Figures and legends

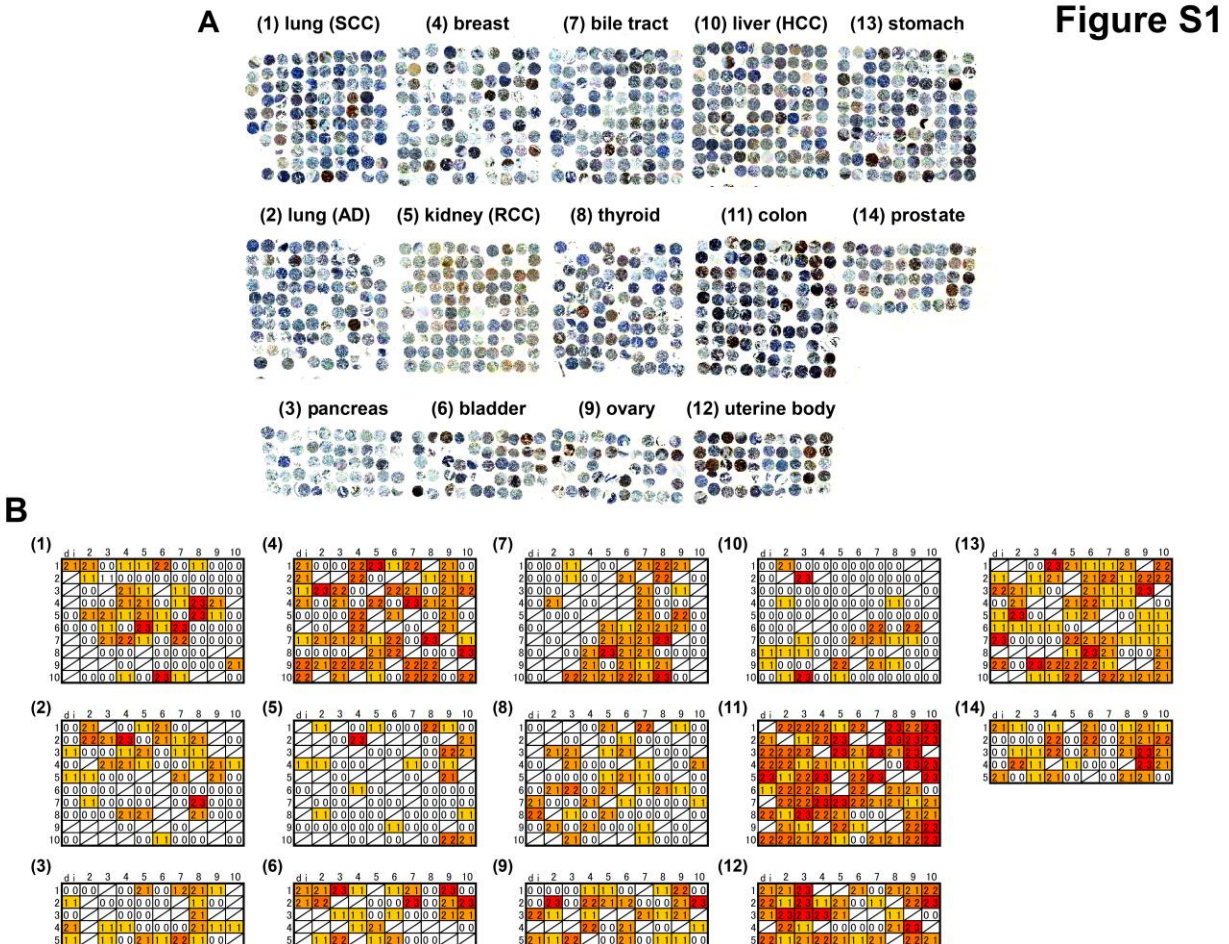


Figure S1. Expression of α 3NaK in human cancer tissues, Related to Fig. 1.

(A) Expression of α 3NaK in human tissue microarrays of multiple cancers. Each group has either 100 or 50 cores from 1 cancer type. A total of 1150 cases from 14 different cancer types are included. Original pictures were shown.

(B) The criteria for the staining were scored as follows: distribution score was scored as 0 (0%), 1 (1–50%), and 2 (51–100%) to indicate the percentage of positive cells in all tumor cells present in one tissue (see left side in each core). The intensity of the signal (intensity score) was scored as 0 (no signal), 1 (weak), 2 (moderate), and 3 (marked) (see right side of each core). The expression score was obtained by adding the distribution and intensity scores. Tissues whose expression score is more than 2 were regarded as positive (colored cores). Shaded cores indicate the tissues with fewer numbers of tumor cells, necrotic changes, and uncertain histology.

Figure S2

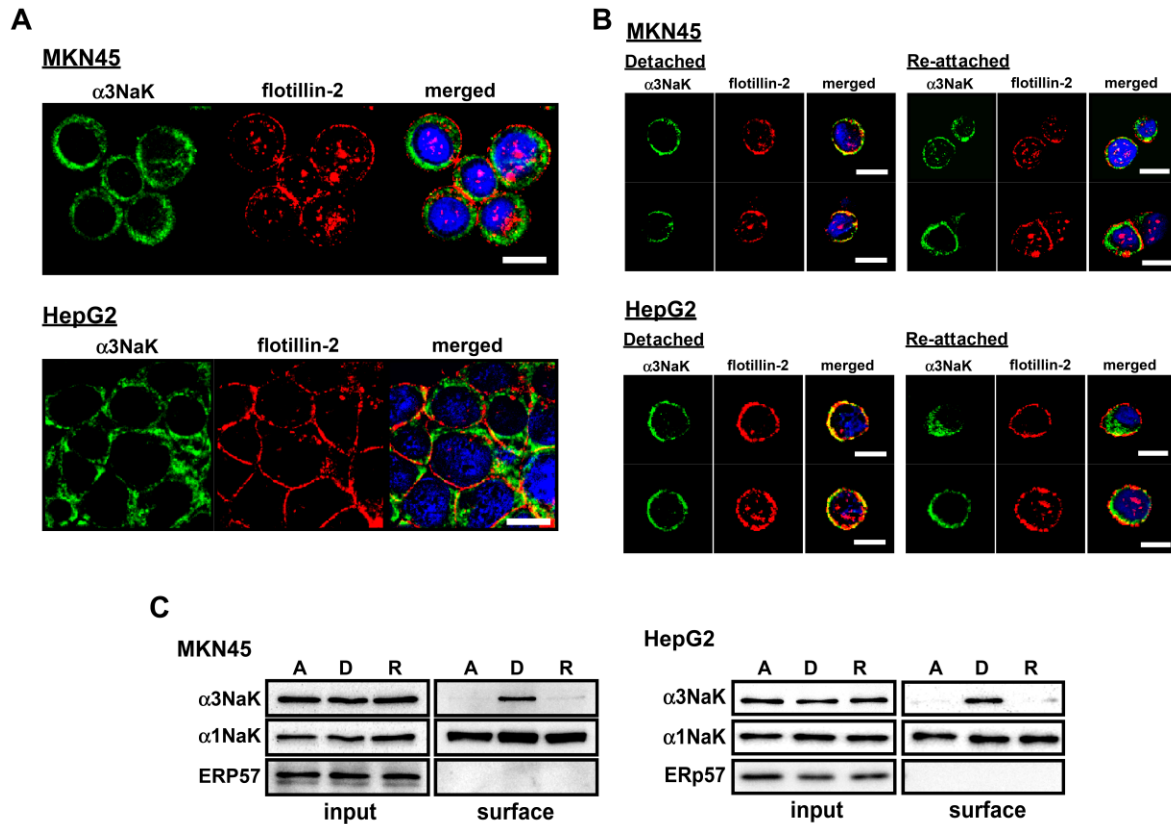


Figure S2. Translocation of α 3NaK to the PM in MKN45 and HepG2 cells, Related to Fig. 1. (A) Immunocytochemistry using antibodies for α 3NaK and flotillin-2 was performed in attached MKN45 and HepG2 cells. Scale bars, 10 μ m. (B) Immunocytochemistry using antibodies for α 3NaK and flotillin-2 was performed in detached and re-attached MKN45 and HepG2 cells. Cells were detached by the treatment with 0.25% trypsin plus 10 mM EDTA. Scale bars, 10 μ m. (C) Western blots of α 3NaK, α 1NaK, and ERp57 in biotinylation samples (surface) and total lysates (input) of attached (A), detached (D), and re-attached (R) MKN45 and HepG2 cells.

Figure S3

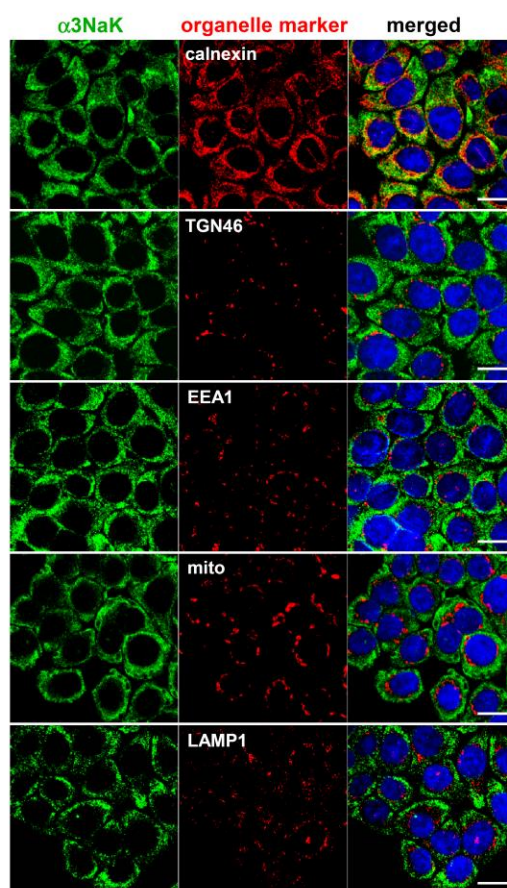


Figure S3. Fluorescent images of $\alpha 3NaK$ and organelle markers in attached HT-29 cells, Related to Fig. 1.

Immunocytochemistry using antibodies for $\alpha 3NaK$ and organelle markers: calnexin (ER), TGN46 (Golgi body), EEA1 (endosome), MitoTracker (mitochondria), and LAMP1 (lysosome) in attached HT-29 cells. Scale bars, 10 μm .

Figure S4

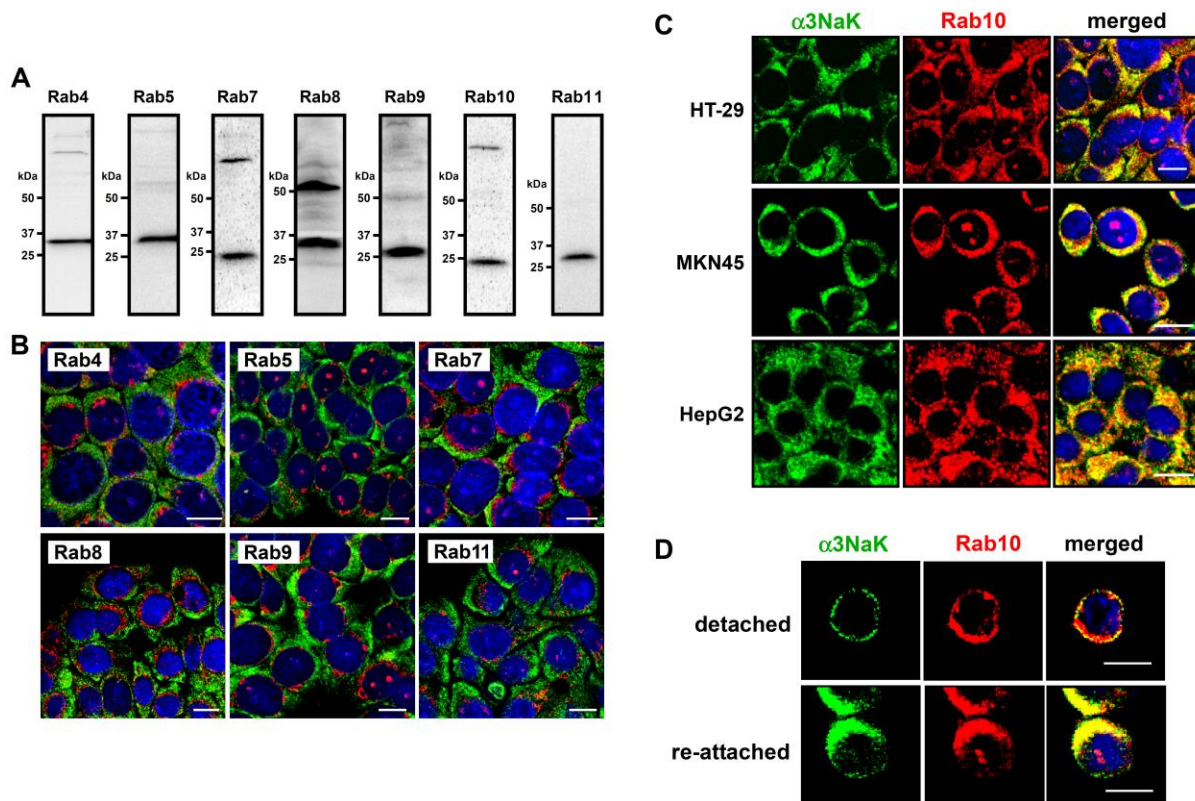


Figure S4. Expression and localization of Rab proteins in human cancer cells, Related to Fig. 1.

(A) Expression of Rab4, 5, 7, 8, 9, 10, and 11 in HT-29 cells.

(B) Fluorescent images of α 3NaK (green) and Rab4, 5, 7, 8, 9, or 11 (red) in attached HT-29 cells. Scale bars, 10 μ m.

(C) Fluorescent images of α 3NaK and Rab10 in attached HT-29, MKN45, and HepG2 cells. Scale bars, 10 μ m.

(D) Fluorescent images of α 3NaK and Rab10 in detached and re-attached HT-29 cells. Scale bars, 10 μ m.

Figure S5

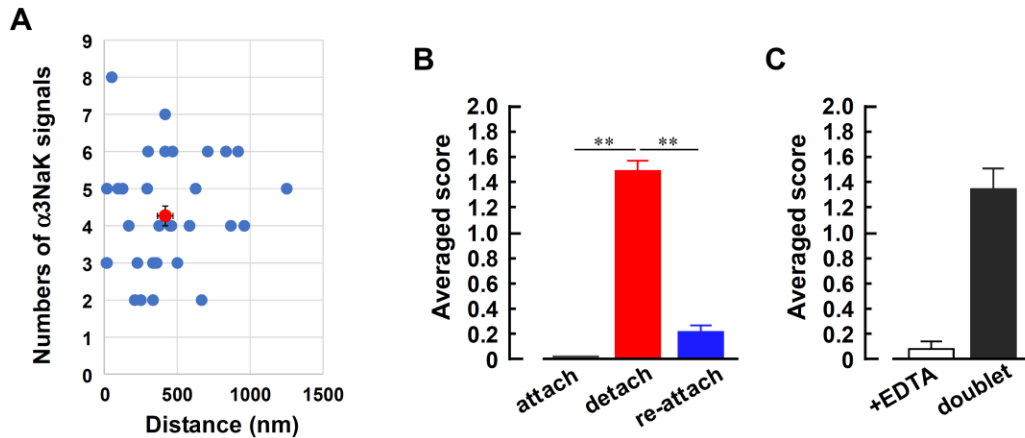


Figure S5. Quantification of the localization of $\alpha 3\text{NaK}$ in HT-29 cells, Related to Fig. 1.

(A) Numbers of $\alpha 3\text{NaK}$ in each assembly and distance of the assembly from the PM was quantified in electron microscopy of HT-29 cells. Thirty-three assemblies were examined. Red circle shows mean values \pm s.e.m.

(B) Distribution of $\alpha 3\text{NaK}$ was scored as 0 (cytoplasm), 1 (both cytoplasm and PM), and 2 (PM) in attached cells ($n = 50$), detached cells ($n = 75$), and re-attached cells ($n = 45$) in Figures 1F and 1H. Average scores were calculated in attached, detached, and re-attached cells. **, $p < 0.01$.

(C) Distribution of $\alpha 3\text{NaK}$ was scored as 0 (cytoplasm), 1 (both cytoplasm and PM), and 2 (PM) in Figures 1K (+EDTA; $n = 23$) and 1L (doublet; $n = 23$). Average scores were calculated.

Figure S6

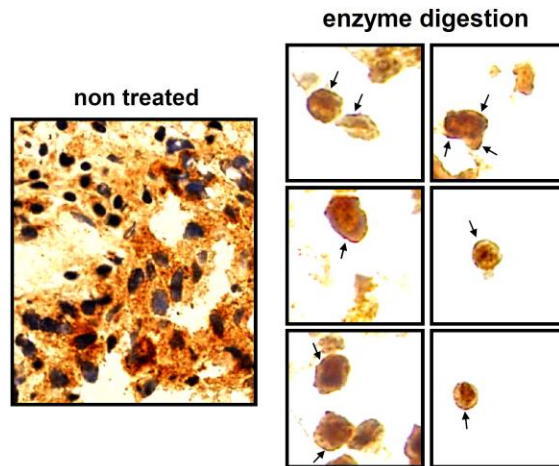


Figure S6. Translocation of $\alpha 3\text{NaK}$ to the PM in enzyme-digested floating human cancer cells, Related to Fig. 1.

Localization of $\alpha 3\text{NaK}$ was examined in human colon cancer tissues (patient No. 4) with or without enzyme digestion (collagenase and actinase E for 30 min at 37°C). Arrows indicate the localization of $\alpha 3\text{NaK}$ at the PM in isolated single cancer cells.

Figure S7

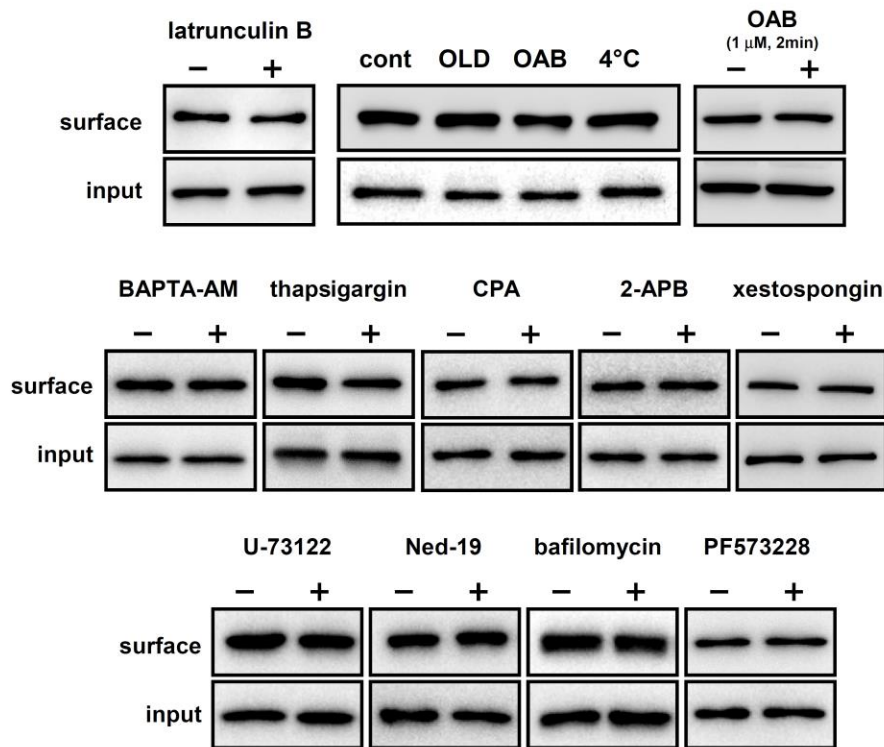


Figure S7. Surface expression of $\alpha 1\text{NaK}$ in HT-29 cells, Related to Fig. 1.

Western blots using an anti- $\alpha 1\text{NaK}$ antibody in the biotinylation samples (surface) and total lysates (input) of detached HT-29 cells. Effect of latrunculin B (10 μM ; 1h), oleandrin (OLD; 1 μM , 1 h), ouabain (OAB; 1 μM , 1 h or 2 min), cooled bath solution ($\sim 4^\circ\text{C}$), BAPTA-AM (100 μM , 30 min), thapsigargin (10 μM , 1 h), CPA (30 μM , 1 h), 2-APB (100 μM , 1 h), xestospongine C (4 μM , 1 h), U-73122 (5 μM , 10 min), Ned-19 (100 μM , 30 min), bafilomycin A1 (100 nM, 1 h), or PF573228 (500 nM, 1 h) on the surface expression level of $\alpha 1\text{NaK}$ in detached HT-29 cells.

Figure S8

	Ab (-)	Ab (+)
α 3NaK	294.99	1536.93
β 1NaK	ND	208.82
β 2NaK	ND	ND
β 3NaK	ND	ND

Figure S8. β -isoform associated with α 3NaK, Related to Fig. 1.

Expression scores of Na⁺,K⁺-ATPase α 3- (α 3NaK), β 1- (β 1NaK), β 2- (β 2NaK), and β 3-isoforms (β 3NaK) in the shotgun mass spectrometry analysis using immunoprecipitated samples with (Ab+) or without (Ab-) an anti- α 3NaK antibody. ND; not detected.

Figure S9

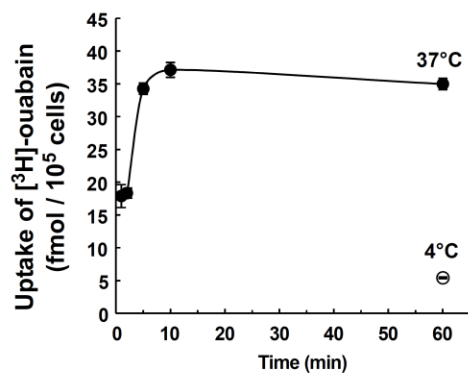


Figure S9. Permeability of ouabain across the PM of the cancer cells, Related to Fig. 1.

The [³H]-ouabain uptake into HT-29 cells was measured at 37°C (1, 2, 5, 10, and 60 min) or 4°C (60 min).

Figure S10



Figure S10. Localization of SERCA2 in HT-29 cells, Related to Fig. 4.
Fluorescent images of $\alpha 3\text{NaK}$ (green) and SERCA2 (red) in attached HT-29 cells. Scale bar, 10 μm .

Figure S11

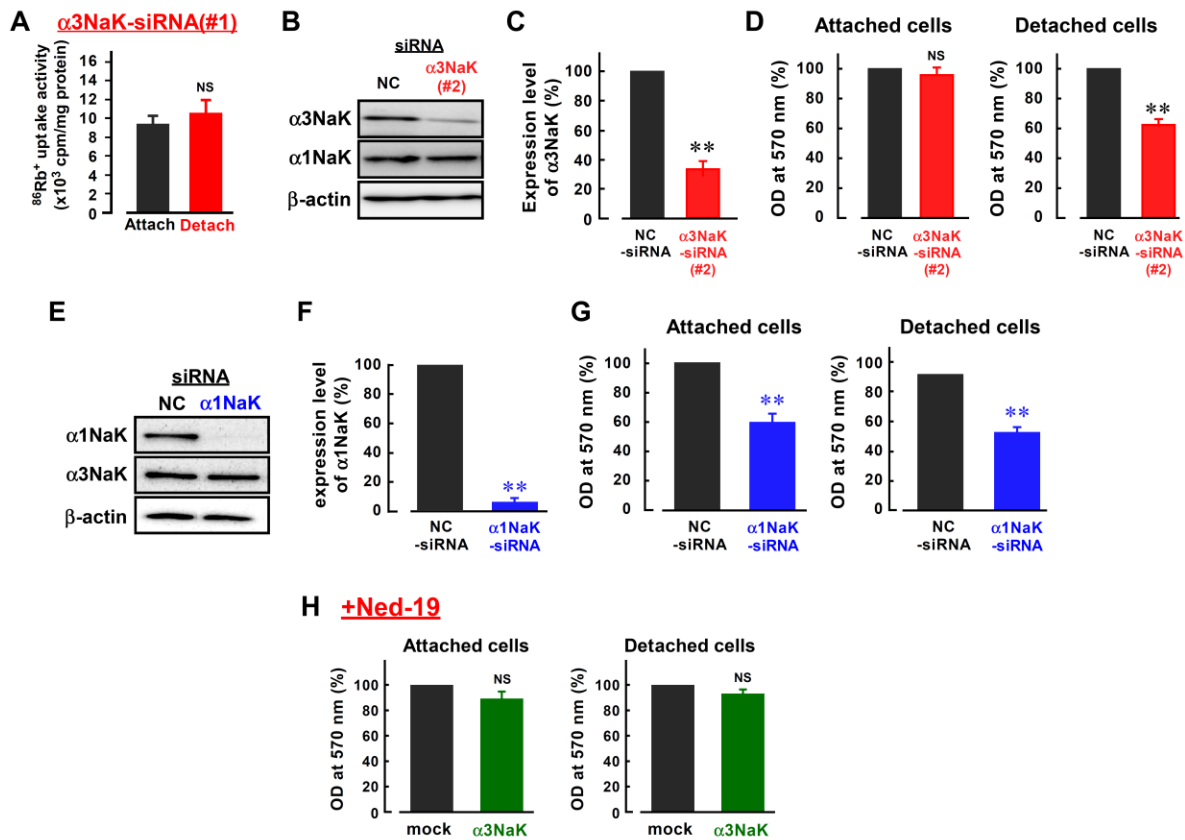


Figure S11. Effects of $\alpha 3\text{NaK}$ - and $\alpha 1\text{NaK}$ -siRNAs and Ned-19 on the viability of cancer cells, Related to Fig. 6.

(A) Effect of $\alpha 3\text{NaK}$ -siRNA (#1) on the $^{86}\text{Rb}^+$ uptake activity in attached and detached HT-29 cells. (n = 6). NS, $p > 0.05$.

(B) Effect of $\alpha 3\text{NaK}$ -siRNA (#2) on expression of $\alpha 1\text{NaK}$, $\alpha 3\text{NaK}$, and β -actin in HT-29 cells. The cells transfected with siRNA for $\alpha 3\text{NaK}$ (#2) or NC-siRNA were used.

(C) Effect of $\alpha 3\text{NaK}$ -siRNA (#2) on expression level of $\alpha 3\text{NaK}$ in HT-29 cells. The cells transfected with $\alpha 3\text{NaK}$ -siRNA (#2) or NC-siRNA were used. The expression level of $\alpha 3\text{NaK}$ in cells transfected with NC-siRNA was normalized as 100 % (n = 3). **, $p < 0.01$.

(D) Effect of $\alpha 3\text{NaK}$ -siRNA (#2) on cell viability of attached and detached HT-29 cells. The cells transfected with $\alpha 3\text{NaK}$ -siRNA (#2) or NC-siRNA were used (n = 4). **, $p < 0.01$. NS, $p > 0.05$.

(E) Effect of $\alpha 1\text{NaK}$ knock down on expression of $\alpha 3\text{NaK}$, and β -actin in HT-29 cells. The cells transfected with siRNA for $\alpha 1\text{NaK}$ ($\alpha 1\text{NaK}$ -siRNA) or NC-siRNA were used.

(F) The expression level of $\alpha 1\text{NaK}$ in cells transfected with $\alpha 1\text{NaK}$ -siRNA was compared with that transfected with NC-siRNA. (n = 7). **, $p < 0.01$.

(G) Effect of $\alpha 1\text{NaK}$ knock down on cell viability of attached and detached HT-29 cells. (n = 5). **, $p < 0.01$.

(H) Effect of Ned-19 (NAADP inhibitor) on cell viability of the colon 38 cells exogenously expressing $\alpha 3\text{NaK}$. The cells transfected with mock and $\alpha 3\text{NaK}$ were used. The cells were treated with 100 μM Ned-19 for 30 min. (n = 6). NS, $p > 0.05$.

Figure S12

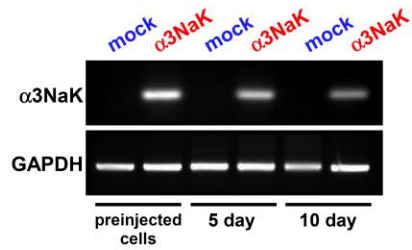


Figure S12. Expression of $\alpha 3NaK$ mRNA in tumor tissues, Related to Fig. 7.

Expression of exogenous $\alpha 3NaK$ in the cDNAs prepared from preinjected cells and tumor tissues 5 or 10 days after injection was examined by RT-PCR. The expression of GAPDH was monitored as a loading control.

Transparent Methods

Cell culture

HT-29 cells were maintained in DMEM (Wako Pure Chemical Industries). MKN-45 cells were in RPMI-1640 (Wako). HepG2 cells were in MEM (Sigma-Aldrich). Colon 38 cells were in DMEM-F12 (Wako). All media were supplemented with 100 units/ml penicillin (Invitrogen), 100 µg/ml streptomycin (Invitrogen), and 10% FBS (Nichirei).

Plasmid construction and transfection

The entire α 3NaK gene (accession number; NM_152296.4) was amplified by PCR using KOD-Plus DNA polymerase and the following primers (sense primer: 5'-ACGGAATTCATGGGGGACAAAGAAAGATGACA-3', and anti-sense primer: 5'-GATCTCGAGTCAGTAGTAGGTTTCCTTCTCCACC-3'). Full-length cDNA encoding human α 3NaK was inserted into the pcDNA4/His vector (Invitrogen) by using BamHI and EcoRI restriction sites. Colon 38 cells were transfected with the vector by using jetPRIME (PolyPlus-transfection) and cultured for 24 h.

Human tissue procurement

Human cancer tissues and adjacent non-tumor tissues, and peritoneal fluids were obtained from Japanese patients in accordance with the recommendations of the Declaration of Helsinki and with ethics committee approval of the University of Toyama (No. 22-45 and 29-85). Informed consent was obtained from all patients at Toyama University Hospital. No donor organs were obtained from executed prisoners or other institutionalized persons. Age (years) and sex (M or F) of the patient, location of each carcinoma, and stage of the carcinoma according to TNM clinical

classification (I, II, III or IV) are No. 1, (74, F, ascending colon, stage IIIa), No. 2 (59, M, gastric body, stage IV), No. 3, (65, M, transverse colon, stage IV), No. 4 (80, M, rectum, stage II).

Animal studies

Six-week-old specific pathogen-free female C57BL/6 mice were purchased from Japan SLC. All experimental procedures were in accordance with the Guide for Care and Use of Experimental Animals of the University of Toyama.

Colon 38 cells (3×10^6 cells) were inoculated into the subcutaneous tissue of the abdominal skin using a Hamilton syringe and 25-gauge needle. After implantation for 5 or 10 days, tumors were harvested from euthanized mice and were weighed. Total RNA was isolated from the tumors and was reverse-transcribed with Superscript III reverse transcriptase (Invitrogen). The expression of $\alpha 3\text{NaK}$ was assessed by RT-PCR of the cDNA using Platinum Taq (Invitrogen), sense primer (5'-GGCTAGCATGACTGGTGGA-3'), and antisense primer (5'-TTCCGGCAGACCTCTTCCAC-3').

In *in vivo* metastasis assay, colon 38 cells (1×10^6 cells) were injected into the tail vein of mice. The animals were sacrificed 7 days later and lungs were excised and processed for total RNA extraction. Total RNA was extracted by the SV Total RNA Isolation System (Promega) and transcribed into cDNA using random primers and ReverTra Ace reverse transcriptase (Toyobo). Quantitative real-time PCR experiments were performed by using Luna Universal Master Mix (New England Biolabs) and an Mx3000p real-time PCR thermocycler (Agilent Technologies, Santa Clara, CA). The following thermal conditions were used: an initial denaturation of 95°C for 1 min and the next 45 cycles of 95°C for 15 s and 60°C for 30 s. The sense primer (5'-CACTATAGGGAGACCCAAGCTG-3') and antisense primer (5'-

GCTGTCCACCAGTCATGCTA-3') were used to assess exogenous expression of the pcDNA4 vector in mouse lung.

RNA interference

Cells (1×10^6 cells) were transfected with 2 μ g of stealth RNAi siRNA for α 1NaK (HSS181499), α 3NaK (#1; HSS181511 and #2; HSS100797), SERCA3 (HSS181578), and stealth RNAi negative control high GC duplex (Invitrogen) via Amaxa nucleofection using solution R (program W-017). Cells were then cultured in growth medium for 48 or 72 h.

Biotinylation of attached and detached cells

Attached cells (2 days after plating) and re-attached cells (60 min after re-plating) were washed with PBS, cell surface proteins were labeled with 0.5 mg/ml sulfo-NHS-biotin (Pierce) in PBS++ (PBS with 1 mM $MgCl_2$ and 1 mM $CaCl_2$) for 30 min at 37°C. In the assay for detached cells, the cells were harvested with 0.25 % trypsin plus EDTA or 10 mM EDTA, then incubated for 30 min at 37°C in the culture medium with agitation. Detached cells were labeled with 0.5 mg/ml sulfo-NHS-biotin in PBS++ by rotating for 30 min at 37°C. Reactions were quenched with PBS++ containing 50 mM glycine and 2 mg/ml BSA and the cells were washed with PBS++. Then, the cells were lysed in the lysis buffer (150 mM NaCl, 50 mM Tris-HCl (pH 7.4), 0.5 mM EDTA, 1% Triton X-100, and protease inhibitors). The biotinylated proteins were isolated by incubating cell lysate with immobilized avidin beads (Sigma-Aldrich) for 12 h at 4°C. The beads were washed with lysis buffer, and the bound proteins were eluted with the SDS sample buffer (62.5 mM Tris, pH 6.8, 10% glycerol, 2% SDS, 2% β -mercaptoethanol, and 0.01% bromphenol blue) for 30 min at 37°C. The biotinylated samples were detected by Western blotting.

Western blotting

Western blotting was performed as previously described (Fujii et al., 2009). The signals were visualized with Pierce Western blotting substrate (Thermo Fisher Scientific) and Western Lightning ECL Pro (PerkinElmer). To quantify the chemiluminescence signals on the membranes, a FujiFilm's LAS-4000 system (FujiFilm) was used. Anti- α 1NaK (1:5,000), α 3NaK (1:2,000), Rab proteins (1:1,000), flotillin-2 (1:5,000), β -actin (1:5,000), myosin IIA (1:5,000), Xpress (1:5,000), SERCA1 (1:1,000), SERCA2 (1:10,000), SERCA3 (1:5,000), ERp57 (1:5,000), pAMPK α (1:2,000), and AMPK α (1:2,000) were used as primary antibodies. Horseradish peroxidase-conjugated anti-rabbit IgG and anti-mouse IgG (Millipore, 1:5,000) were used as secondary antibodies. Human skeletal muscle lysate was obtained from Takara Bio.

Immunocytochemistry

Detached cells were embedded in the O.C.T. compound (Sakura) and were cut at 6 μ m. The sections were fixed in ice-cold methanol for 3 min at room temperature. Attached cells cultured on coverslips were fixed with ice-cold methanol for 3 min and permeabilized with PBS containing 0.3% Triton X-100 and 0.1% BSA for 15 min at room temperature. Non-specific binding of antibodies was blocked by using the solution containing 20 mM phosphate buffer (pH 7.4), 450 mM NaCl, 16.7% goat serum, and 0.3% Triton X-100. The cells were incubated with primary antibodies (1:100) for 15 h at 4°C, and then with Alexa Fluor 488-conjugated anti-mouse IgG and Alexa Fluor 546-conjugated anti-rabbit IgG antibodies (Thermo Fisher Scientific, 1:100) for 1 h at room temperature. DNA was visualized using DAPI (Dojindo, 1:1,000). Immunofluorescence images were visualized by using a Zeiss LSM 700 or 780 laser scanning confocal microscope.

Human tissue microarrays

Human tissue microarrays were constructed as previously described (Fukuoka et al., 2004). Four- μ m-thick sections were cut using an adhesive-coated tape and transferred on the slide glass through the water tab. After the complete dry, the adhesive tape was removed in the coplin jar with xylene. The slides were then immunohistochemically stained as described below. The signal of α 3NaK was scored by three pathologists into positive and negative groups as shown in Figure S1. Tissue cores of the slide with fewer numbers of tumor cells, necrotic changes, and uncertain histology were excluded from the analysis. Human cancer tissues were obtained from Japanese patients in accordance with the recommendations of the Declaration of Helsinki and with ethics committee approval of the University of Toyama (No. 24-58).

Immunohistochemistry

Formalin-fixed and paraffin-embedded tissues were cut into 4- μ m-thick sections. The sections were deparaffinized with xylene and rehydrated through graded alcohols into water. Heat-induced epitope retrieval was performed using the Decloaking Chamber (DAKO, Kyoto, Japan), in which tissues were heated to 125°C and cooled to 90°C in Tris/EDTA buffer at pH 9 (Target Retrieval Solution; DAKO). After heat-induced epitope retrieval treatment, endogenous peroxidase was blocked with Peroxidase-Blocking Solution (DAKO) for 10 min. Then the sections were incubated with anti- α 3NaK antibody (1:200) for 15 h or anti-CEA (1:100) for 30 min. The primary antibody was then incubated with EnVision+ Dual Link system (DAKO). Subsequently, the reaction products were visualized with DAB+ (DAKO). Nuclei were lightly counterstained with Mayer's hematoxylin. All procedures were carried out at room temperature.

Immunoelectron microscopy

High-pressure freezing (HPF) was performed as previously described (Sawaguchi et al., 2008). HT-29 cells were cultured on sterilized 10- μ m-thin stainless discs in 24-well plates. Prior to cryofixation by HPF, two stainless discs with the cultured cells were assembled with a one-hole copper grid as a spacer ring (Nisshin EM) and type B aluminium planchettes (Engineering Office M. Wohlwend). This assembly was immediately frozen at 2100 bars in an HPF machine (HPM 010; BAL-TEC) and rapidly transferred to LN₂ for storage until required for further processing of freeze substitution. Ultrathin sections (60-80 nm thick) were picked up on 150-mesh gold grids coated with Formvar film and treated with 1% BSA in PBS for 10 min to block non-specific binding. Then the sections were incubated with anti- α 3NaK antibody (1: 500) at 4°C for 15 h. After washing with PBS, the sections were treated with biotinylated goat anti-mouse IgG at room temperature for 60 min. Then, the sections were incubated with CG conjugated goat anti-biotin (diluted with 1% BSA in PBS) at room temperature for 30 min. After washing with distilled water and drying, the sections were contrasted by the KMnO₄-UA/Pb staining as previously described (Sawaguchi et al., 2001).

Isolation of cancer cells from human cancer tissues

To isolate single cancer cells from human colorectal cancer tissues, the tissues were digested with MEM containing 10% FBS, 200 units/ml collagenase (Wako), and 667 tyrosine units/ml actinase E (Kaken Pharmaceutical) for 30 min at 37°C. The digested solution was centrifuged at 200 xg for 5 min and the pellet was embedded in the O.C.T. compound.

Measurement of ouabain-sensitive $^{86}\text{Rb}^+$ uptake

HT-29 cells (2×10^6 cells) were grown on 6-well plates for 24 h. Cells were preincubated in DMEM containing 10 μM DIOA, 100 μM furosemide, and 10 μM ouabain for 10 min at 37°C. After the pre-exposure, the cells were treated with the DMEM containing 10 μM DIOA, 100 μM furosemide, $^{86}\text{RbCl}$ (6×10^6 cpm/sample), and 10 μM ouabain for 10 min at 37°C. In control, ouabain was omitted. Incubation was stopped by cooling on ice, and plates were washed with an ice-cold DMEM, and the radioactivity was measured by liquid scintillation. When the medium of detached cells was changed, the cells were centrifuged at 300 x g for 3 min and the supernatants were discarded.

Measurement of uptake of [^3H]-ouabain into HT-29 cells

HT-29 cells (4×10^5 cells) were grown on 24-well plates for 24 h. The cells were incubated with DMEM containing 1 μM ouabain (0.1 μM [^3H]-ouabain plus 0.9 μM ouabain) for 1, 2, 5, 10, and 60 min at 37°C or for 60 min at 4°C. Incubation was stopped by cooling on ice. The cells were washed with an ice-cold DMEM, and the radioactivity of them was measured by liquid scintillation.

Electrophysiology

Membrane capacitance in whole-cell patch-clamp recordings was measured using the membrane test tool of Clampex software (version 9.2; Axon Instruments) in an Axopatch 200B amplifier (Axon Instruments). Clampfit software (version 9.2; Axon Instruments) was used for data analysis. The pipette resistances were around 2-5 M Ω . The pipette solution contained 7 mM NaCl, 133 mM potassium aspartate, 3 mM MgCl₂, 0.062 mM CaSO₄, 0.1 mM EGTA, 10 mM HEPES, and 2 mM ATP (pH 7.3). The bathing solution contained 136 mM NaCl, 4 mM KCl, 1 mM sodium aspartate, 1 mM MgCl₂, 1 mM CaSO₄, 7 mM Tris, 10 mM HEPES, and 5 mM EDTA (pH 7.3).

Measurement of $[Ca^{2+}]_i$

Fluo-4-AM (Dojin Chemicals) was loaded into HT-29 cells cultured on glass-bottom dishes for 12 h; the cells were treated with 5 μ M Fluo-4/AM for 30 min at 37°C. The cells were washed and replaced with the Ca^{2+} -free solution containing 145 mM NaCl, 4.5 mM KCl, 1 mM $MgCl_2$, 10 mM HEPES, and 5 mM EDTA (pH 7.3). Fluorescence of Fluo-4 was monitored by using the confocal laser scanning microscope (TCS-SP5; Leica).

Cell viability

Cell viability was assessed by MTT cell proliferation assay kit (Cayman). HT-29 and colon 38 cells were harvested, counted, and aliquoted at equal numbers (1×10^5 cells), and then incubated for 6 h at 37°C. The cells were mixed with MTT reagents and incubated for 3 h at 37°C. Then, they were centrifuged at 300 x g for 5 min, the supernatants were discarded. The pellets of cells were dissolved in the crystal dissolving solution. The absorbance was measured at 570 nm using a microplate reader.

Caspase 3/7 assay

Cell apoptosis was evaluated by Caspase-Glo 3/7 Assay System (Promega). HT-29 and colon 38 cells were harvested, counted, and aliquoted at equal numbers (1×10^4 cells), and then incubated for 3 h at 37°C. The cells were mixed with Caspase-Glo 3/7 Assay reagent and incubated for 1 h at 37°C. Then, the luminescence was measured with a microplate reader (Filter Max F5).

Measurement of intracellular ROS level

Intracellular ROS level was detected using the fluorescent probe carboxy-H₂DCFDA (Thermo Fisher Scientific). Cells were incubated with culture medium containing 100 μ M carboxy-H₂DCFDA for 60 min at 37°C. The cells were washed twice with PBS, incubated with 5 mM EDTA in DMEM for 10 min, and then placed in a microplate reader (Filter Max F5). Cells were detached by pipetting and fluorescence was sequentially measured at 485 nm (excitation) and 538 nm (emission).

Quantification and statistical analysis

Results are shown as means \pm s.e.m. Differences between groups were analyzed by one-way ANOVA. A comparison between the two groups was made by using Fisher's exact test and Student's *t*-test. Statistically significant differences were assumed at $p < 0.05$.

STAR Methods

KEY RESOURCES TABLE

REAGENT or RESOURCE	SOURCE	IDENTIFIER
Antibodies		
Mouse monoclonal anti- α 3NaK (clone: XVIF9-G10)	Affinity BioReagents	Cat # MA3-915; RRID: AB_2274447
Mouse monoclonal anti- α 1NaK (clone: C464.6)	Santa Cruz	Cat # sc-21712 RRID: AB_626713
Rabbit polyclonal anti-Lamp1	Santa Cruz	Cat # SC5570 RRID: AB_2249779
Rabbit monoclonal anti-calnexin (clone: C5C9)	Cell Signaling Technology	Cat # 2679S RRID: AB_2228381
Rabbit monoclonal anti-EEA1 (clone: C45B10)	Cell Signaling Technology	Cat # 3288S RRID: AB_2096811
Rabbit polyclonal anti-Rab4	Cell Signaling Technology	Cat # 2167S RRID: AB_2253579
Rabbit polyclonal anti-Rab5	Cell Signaling Technology	Cat # 2143S RRID: AB_823625
Rabbit polyclonal anti-Rab7	Cell Signaling Technology	Cat # 2094S RRID: AB_2300652
Rabbit polyclonal anti-Rab9	Cell Signaling Technology	Cat # 2095S RRID: AB_2175603
Rabbit monoclonal anti-Rab11 (clone: D4F5)	Cell Signaling Technology	Cat # 5589S RRID: AB_10693925
Mouse monoclonal anti-pAMPK α (Thr172) (clone: 40H9)	Cell Signaling Technology	Cat # 2535 RRID: AB_331250

Rabbit monoclonal anti-AMPK α (clone: D5A2)	Cell Signaling Technology	Cat # 4811 RRID: AB_11178532
Rabbit polyclonal anti-Rab8	Sigma-Aldrich	Cat # R5530 RRID: AB_2175306
Rabbit polyclonal anti-Rab10	Sigma-Aldrich	Cat # R8906 RRID: AB_2173447
Rabbit polyclonal anti-flotillin-2	Sigma-Aldrich	Cat # F1680 RRID: AB_1078895
Mouse monoclonal anti- β -actin (clone: AC-74)	Sigma-Aldrich	Cat # A5316 RRID: AB_476743
Rabbit polyclonal anti-myosin IIA	Sigma-Aldrich	Cat # M8064 RRID: AB_260673
Rabbit polyclonal anti-SERCA3	Aviva Systems Biology	Cat # ARP46580 RRID: AB_2045026
Rabbit monoclonal anti-SERCA1 (clone: EPR7321)	Abcam	Cat # ab133275 RRID: AB_11157766
Rabbit monoclonal anti-SERCA2 (clone: EPR9392)	Abcam	Cat # ab150435
Rabbit polyclonal anti-TGN46	Abcam	Cat # ab50595 RRID: AB_2203289
Mouse monoclonal anti-ERp57 (clone: MaP.Erp57)	Stressgen	Cat # SPA-725-F RRID: AB_1193493
Mouse monoclonal anti-Xpress	Invitrogen	Cat # R910-25 RRID: AB_2556552
Mouse monoclonal anti-CEA (clone: II-7)	DAKO	Cat # GA62261-2
Bacterial and Virus Strains		
ElectroMAX DH10B Cells	Invitrogen	Cat # 18290-015
Biological Samples		
Human colon cancer tissues	University of Toyama	N/A
Human gastric cancer tissues	University of Toyama	N/A
Human skeletal muscle lysate	Takara Bio.	Cat # PK-AB718-1375
Human tissue microarray	University of Toyama	N/A
Chemicals, Peptides, and Recombinant Proteins		
Ouabain	Sigma-Aldrich	Cat # O3125
2-APB	Sigma-Aldrich	Cat # D9754
PF573228	Sigma-Aldrich	Cat # PZ0117
CPA	Sigma-Aldrich	Cat # C1530
DIOA	Sigma-Aldrich	Cat # D129
Collagen from human placenta	Sigma-Aldrich	Cat # C7521
Fibronectin from human plasma	Sigma-Aldrich	Cat # F2006
Oleandrin	Wako	Cat # 06069
Latrunculin B	Wako	Cat # 129-05101
Thapsigargin	Wako	Cat # 209-17281
BAPTA-AM	Wako	Cat # 348-05451
Xestopongin C	Wako	Cat # 244-00721
Bafilomycin A1	Wako	Cat # 554-29211
U-73122	Enzo Life Sciences	Cat # BML-ST391-0005
Ned-19	R&D Systems	Cat # 3954/10
DAPI	Dojindo	Cat # 340-07971
Collagenase	Wako	Cat # 032-22364
Actinase E	Kaken Pharmaceutical	Cat # KA-001
⁸⁶ RbCl	PerkinElmer	Cat # NEZ072
[³ H]-ouabain	Muromachi Kagaku	Cat # ART1322
Superscript III reverse transcriptase	Invitrogen	Cat # 18080-044
ReverTra Ace reverse transcriptase	Toyobo	Cat # TRT-101

Platinum Taq	Invitrogen	Cat # 10966018
Critical Commercial Assays		
JetPRIME	PolyPlus-transfection	Cat # 114-15
Amaxa Cell Line Nucleofector® Kit R	Lonza	Cat # VCA-1001
Western Lightning ECL Pro	PerkinElmer	Cat # NEL120001EA
Pierce Western blotting substrate	Thermo Fisher Scientific	Cat # 32106
Sulfo-NHS-biotin	Pierce	Cat # NI-21335
MTT cell proliferation assay kit	Cayman	Cat # 10009365
Caspase-Glo 3/7 Assay System	Promega	Cat # G8090
carboxy-H ₂ DCFDA	Thermo Fisher Scientific	Cat # C13293
SV Total RNA Isolation System	Promega	Cat # Z3100
Luna Universal Master Mix	New England Biolabs	Cat # M3003S
Fluo-4-AM	Dojindo	Cat # F312
Experimental Models: Cell Lines		
Human: HT-29 cells	ATCC	Cat # HTB-38
Human: MKN-45 cells	JCRB Cell Bank	Cat # JCRB0254
Human: HepG2 cells	RIKEN Cell Bank	Cat # RCB1648
Experimental Models: Organisms/Strains		
Mouse: C57BL/6	Japan SLC	C57BL/6NCrSlc
Oligonucleotides		
Stealth RNAi siRNA for α 1NaK	Invitrogen	Cat # HSS181499
Stealth RNAi siRNA for α 3NaK	Invitrogen	Cat # HSS181511
Stealth RNAi siRNA for α 3NaK	Invitrogen	Cat # HSS100797
Stealth RNAi siRNA for SERCA3	Invitrogen	Cat # HSS181578
Stealth RNAi negative control high GC duplex	Invitrogen	Cat # 12935400
Primers for human α 3NaK cloning	This paper	N/A
Primers for checking α 3NaK expression	This paper	N/A
Recombinant DNA		
pcDNA4/His	Invitrogen	Cat # V862-20
Human α 3NaK in pcDNA4/His	This paper	N/A
Software and Algorithms		
ImageJ	ImageJ	https://imagej.nih.gov/ij/
Clampex	Axon Instruments	version 9.2
Clampfit	Axon Instruments	version 9.2
LSM Image Browser	Zeiss	version 3.5
Other		
DMEM	Wako	Cat # 044-29765
RPMI 1640	Wako	Cat # 189-02025
DMEM-F12	Wako	Cat # 048-29785
MEM	Sigma-Aldrich	Cat # M4655
FBS	Nichirei	Cat # 171012
Penicillin/streptomycin	Invitrogen	Cat # 15140

Supplemental References

Fujii, T., Takahashi, Y., Ikari, A., Morii, M., Tabuchi, Y., Tsukada, K., Takeguchi, N., and Sakai, H. (2009). Functional association between K^+ - Cl^- cotransporter-4 and H^+ , K^+ -ATPase in the apical canalicular membrane of gastric parietal cells. *J. Biol. Chem.* *284*, 619-629.

Fukuoka, J., Fujii, T., Shih, J.H., Dracheva, T., Meerzaman, D., Player, A., Hong, K., Settnek, S., Gupta, A., Buetow, K., et al. (2004). Chromatin remodeling factors and BRM/BRG1 expression as prognostic indicators in non-small cell lung cancer. *Clin. Cancer Res.* *10*, 4314-4324.

Sawaguchi, A., Aoyama, F., Ide, S., Goto, Y., and Suganuma, T. (2008). A new device for high-pressure freezing of cultured cell monolayer using 10-micron-thin stainless discs as both culture plate and specimen carrier. *J. Electron Microsc.* *57*, 203-206.

Sawaguchi, A., Ide, S., Goto, Y., Kawano, J., Oinuma, T., and Suganuma, T. (2001). A simple contrast enhancement by potassium permanganate oxidation for Lowicryl K4M ultrathin sections prepared by high pressure freezing/freeze substitution. *J. Microsc.* *201*, 77-83.